

# Cyclic Triaxial Tests of the Bootlegger Cove Formation, Anchorage, Alaska

By POUL V. LADE, RANDALL G. UPDIKE,  
and DAVID A. COLE

A cooperative research project between the  
U.S. Geological Survey and the  
State of Alaska Division of Geological and Geophysical Surveys

U.S. GEOLOGICAL SURVEY BULLETIN 1825

DEPARTMENT OF THE INTERIOR  
DONALD PAUL HODEL, Secretary



U. S. GEOLOGICAL SURVEY  
Dallas L. Peck, Director

Any use of trade names is for descriptive purposes only and does not imply endorsement by the U.S. Geological Survey.

UNITED STATES GOVERNMENT PRINTING OFFICE: 1988

---

For sale by the  
Books and Open-File Reports Section  
U.S. Geological Survey  
Federal Center  
Box 25425  
Denver, CO 80225

**Library of Congress Cataloging-in-Publication Data**

Lade, P.

Cyclic triaxial tests of the Bootlegger Cove Formation, Anchorage, Alaska.

(U.S. Geological Survey bulletin ; 1825)

"A cooperative research project between the U.S. Geological Survey and the State of Alaska Division of Geological and Geophysical Surveys."

Bibliography: p.

Supt. of Docs. no.: I 19.3:1825

1. Soils—Alaska—Anchorage Region—Testing. 2. Shear strength of soils—Testing. 3. Bootlegger Cove Formation (Alaska) I. Updike, Randall G. II. Cole, David A. III. Alaska. Division of Geological and Geophysical Surveys. IV. Title. V. Series.

QE75.B9 no. 1825 557.3 s [624.1'762]

87-600446

[TA710.3A4]

# CONTENTS

Glossary of symbols used	VI
Abstract	1
Introduction	1
Scope	1
Acknowledgments	2
Regional geologic history	2
Tectonic setting	2
Quaternary history	3
Engineering geologic facies of the Bootlegger Cove Formation	3
Geologic history of the site	4
Static engineering characterization of the site	7
Field sampling and logging	7
Dynamic laboratory testing program	7
Unconsolidated-undrained tests	8
Equipment	8
Testing procedure	8
Consolidated-undrained tests	9
Equipment	9
Testing procedure	9
Cyclic loading tests	10
Equipment	10
Testing procedure	10
Results of laboratory testing	11
Soil index tests	11
Static tests	11
Cyclic loading tests	16
Strength relations for intact specimens	16
Discussion of cyclic stress ratio	18
Strength relations for remolded specimens	18
Comparison of strength relations for intact and remolded specimens	19
Shear moduli	22
Damping ratios	23
Summary and conclusions from laboratory testing	24
References cited	26

## FIGURES

1. Photograph of the Turnagain Heights landslide 2
2. Generalized map showing major faults in the vicinity of Anchorage 3
3. Generalized map showing the location of the sample site 4
4. Map showing the location of boreholes and cross-section lines 4
5. Geologic cross section along line A-A' 5
6. Geologic cross section along line B-B' 6
7. Photograph of triaxial testing equipment used for UU tests 8
8. Photograph of triaxial testing equipment used for static ICU tests 9
9. Photograph of cyclic triaxial testing equipment 10
10. Plasticity chart for samples 11

## FIGURES

11. Graph showing undrained shear strength versus water content derived from UU and ICU tests 14
12. The p-q diagram showing effective normal stress versus maximum shearing stress determined by ICU tests 16
13. Photograph of specimen CT-5 (F.IV) after consolidation and after failure by cyclic loading 17
14. Photograph of specimen CT-3 (F.III) after consolidation and after failure by cyclic loading 18
15. Photograph of specimen CT-4 (F.IV) after consolidation and after failure by cyclic loading 19
- 16-47. Graphs showing:
  16. Peak-to-peak axial strain versus number of cycles for intact samples at  $K_c = 1.0$  22
  17. Cyclic stress ratio from UU tests versus number of cycles for intact specimens at  $K_c = 1.0$  23
  18. Cyclic stress ratio from ICU tests versus number of cycles for intact specimens at  $K_c = 1.0$  24
  19. Maximum axial strain versus number of cycles for intact specimens at  $K_c = 1.5$  25
  20. Maximum axial strain versus number of cycles for intact specimens at  $K_c = 2.0$  26
  21. Cyclic stress ratio from UU tests versus number of cycles for intact specimens at  $K_c = 1.5$  27
  22. Cyclic stress ratio from ICU tests versus number of cycles for intact specimens at  $K_c = 1.5$  28
  23. Cyclic stress ratio from UU tests versus number of cycles for intact specimens at  $K_c = 2.0$  29
  24. Cyclic stress ratio from ICU tests versus number of cycles for intact specimens at  $K_c = 2.0$  30
  25. Cyclic stress ratio from UU tests versus number of cycles for intact specimens at  $K_c = 1.0, 1.5,$  and  $2.0$  31
  26. Peak-to-peak axial strain versus number of cycles for remolded specimens at  $K_c = 1.0$  32
  27. Maximum axial strain versus number of cycles for remolded specimens at  $K_c = 1.5$  33
  28. Maximum axial strain versus number of cycles for remolded specimens at  $K_c = 2.0$  34
  29. Cyclic stress ratio from UU tests versus number of cycles for remolded specimens at  $K_c = 1.0$  35
  30. Cyclic stress ratio from UU tests versus number of cycles for remolded specimens at  $K_c = 1.5$  36
  31. Cyclic stress ratio from UU tests versus number of cycles for remolded specimens at  $K_c = 2.0$  37
  32. Cyclic stress ratio from ICU tests versus number of cycles for remolded specimens at  $K_c = 1.0$  38
  33. Cyclic stress ratio from ICU tests versus number of cycles for remolded specimens at  $K_c = 1.5$  39
  34. Cyclic stress ratio from ICU tests versus number of cycles for remolded specimens at  $K_c = 2.0$  40
  35. Cyclic stress ratio from UU tests versus number of cycles for remolded specimens at  $K_c = 1.0, 1.5,$  and  $2.0$  41
  36. Cyclic stress ratio from ICU tests versus number of cycles for remolded specimens at  $K_c = 1.0, 1.5,$  and  $2.0$  42

## FIGURES

37. A comparison of cyclic stress ratios for intact (UU tests) specimens and remolded (ICU tests) specimens 43
38. A comparison of cyclic stress ratios for intact (estimated ICU tests) and remolded (measured ICU tests) specimens 44
39. Normalized shear moduli for intact specimens using shear strengths from UU tests 45
40. Normalized shear moduli for intact specimens using shear strengths from estimated ICU tests 45
41. Normalized shear moduli for remolded specimens using shear strengths from UU tests 46
42. Normalized shear moduli for remolded specimens using shear strengths from ICU tests 46
43. A comparison of shear moduli versus number of cycles for intact and remolded specimens at  $K_c = 1.0$  47
44. A comparison of shear moduli versus number of cycles for intact and remolded specimens at  $K_c = 1.5$  48
45. A comparison of shear moduli versus number of cycles for intact and remolded specimens at  $K_c = 2.0$  49
46. Damping ratios versus percent strain for intact specimens 50
47. Damping ratios versus percent strain for remolded specimens 51

## TABLES

1. Summary of Atterberg limit and hydrometer tests 12
2. Summary of torvane and UU triaxial tests 13
3. Summary of ICU triaxial tests 15
4. Summary of initial and stress conditions for cyclic tests on intact specimens 20
5. Summary of initial and stress conditions for cyclic tests on remolded specimens 21

## CONVERSION FACTORS

For readers who wish to convert measurements from the metric system of units to the inch-pound system of units, the conversion factors are listed below.

Metric unit	Multiply by	To obtain inch-pound unit
millimeter (mm)	0.03937	inch
centimeter (cm)	0.3937	inch
meter (m)	3.281	foot (ft)
centimeter <sup>2</sup> (cm <sup>2</sup> )	0.1550	inch <sup>2</sup>
centimeter <sup>3</sup> (cm <sup>3</sup> )	0.06102	inch <sup>3</sup>
kilogram (kg)	2.205	pound (lb)
metric ton	1.102	ton, short (2000 lb)
kilogram/centimeter <sup>2</sup> (kg/cm <sup>2</sup> )	14.223	pound/inch <sup>2</sup> (psi)
gram/centimeter <sup>3</sup> (g/cm <sup>3</sup> )	62.43	pound/foot <sup>3</sup> (lb/ft <sup>3</sup> )

GLOSSARY OF SYMBOLS USED

$A$	Activity of clay; PI/percent clay	$S_u$	Undrained shear strength
$A_o$	Initial cross-sectional area of specimen	$t_{50}$	Time to reach 50 percent consolidation
$A_c$	Cross-sectional area of specimen after consolidation	$t_{100}$	Time to reach 100 percent consolidation
$B$	(Measured pore pressure increase)/(applied confining pressure increase)	$U$	Pore pressure
CL	Unified Classification symbol for clay with low plasticity	$U_f$	Pore pressure at failure
CU	Consolidated-undrained (test)	$U_{max}$	Maximum pore pressure
CUPI	Consolidated-undrained cyclic (pulsating) test on intact specimen	UU	Unconsolidated-undrained (test)
CUPR	Consolidated-undrained cyclic (pulsating) test on remolded specimen	$V_o$	Initial volume of specimen
$c_v$	Coefficient of consolidation	$w/c$	Water content
$D$	Damping ratio	$\gamma$	Single-amplitude shear strain
$D_{50}$	Median particle diameter	$\gamma_{wet}$	Wet density
$G$	Shear modulus	$\Delta V_{consol}$	Volume change of specimen due to consolidation
$G_s$	Specific gravity of soil particles	$\Delta \delta_{consol}$	Vertical deformation of specimen due to consolidation
$H_o$	Initial height of specimen	$\epsilon_{1consol}$	Vertical strain of specimen due to consolidation
$H_c$	Height of specimen after consolidation	$\epsilon_V$	Vertical strain at failure
ICU	Isotropically consolidated-undrained (test)	$\epsilon_{1max}$	Maximum vertical strain
$K_c$	Consolidation stress ratio; $\sigma_{1c}/\sigma_{3c}$	$\epsilon_{vconsol}$	Volumetric strain of specimen due to consolidation
LL	Liquid limit	$\sigma_1$	Principal applied stress in triaxial cell
$N$	Number of load cycles applied to specimen	$\sigma_{1c}$	Principal applied stress during consolidation
$N_f$	Number of load cycles to cause failure of specimen	$\sigma_3$	Confining pressure in triaxial cell
$N_{max}$	Maximum number of load cycles applied to specimen	$\sigma_{3c}$	Confining pressure during consolidation
$P_{dp}$	Cyclic (pulsating) deviator load	$\sigma'_{3f}$	Effective confining pressure at failure
PI	Plasticity index; LL - PL	$(\sigma_1 - \sigma_3)_{max}$	Deviator stress
PL	Plastic limit	$(\sigma'_1 / \sigma'_3)_{max}$	Effective stress ratio
$S_p$	Half of cyclic (pulsating) deviator stress; $\sigma_{dp}/2$	$\sigma_{dc}$	Deviator stress during consolidation
$S_r$	Sensitivity; $S_u(intact)/S_u(remolded)$	$\sigma_{dmax}$	Maximum deviator stress applied to specimen; $\sigma_{dc} + \sigma_{dp}$
		$\sigma_{dp}$	Cyclic (pulsating) deviator stress
		$\phi$	Friction angle
		$\phi'$	Effective friction angle

# Cyclic Triaxial Tests of the Bootlegger Cove Formation, Anchorage, Alaska

By Poul V. Lade<sup>1</sup>, Randall G. Updike, and David A. Cole<sup>2</sup>

## Abstract

Earthquake-induced landslides in the Anchorage area have resulted primarily from cohesive soil failures within the Bootlegger Cove Formation. A suite of ten undisturbed samples from various formational facies were tested in an investigation of representative stress-strain and strength properties under static and cyclic loading conditions. A sequence of soil index property tests was followed by unconsolidated-undrained static triaxial tests on intact and remolded specimens, isotropically consolidated-undrained static triaxial tests on remolded specimens, and cyclic triaxial tests on intact and remolded specimens at various consolidation ratios. The intent of this testing program was to "calibrate" the static and dynamic behavior of the cohesive facies of the formation in the previously determined zone of failure. The results indicate that, at higher consolidation stress ratios, higher cyclic stress ratios are required to cause a given amount of strain for a finite number of cycles. Though the evidence is not conclusive, there is an indication that soils remolded in landslide areas have strengths equal to those of soils in areas that have not failed. Sensitivity values determined on these samples are substantially lower than those reported in the literature, which suggests that criteria other than sensitivity must be considered in evaluating the stability of the Bootlegger Cove Formation during earthquakes.

## INTRODUCTION

The City of Anchorage lies within one of the most active tectonic regions of the world and is therefore subjected to frequent seismic events which have magnitudes as great as that of the catastrophic Prince William Sound earthquake of March 27, 1964. Moderate- to large-magnitude earthquakes can be expected to occur in the region within the design life of most major buildings now existing or planned for construction in the city. During

the 1964 earthquake the primary cause of property damage and loss of life in Anchorage was related to ground failure (landslides) that resulted from the intense shaking (fig. 1). These landslides have been attributed to three failure mechanisms: (1) gravity fall along unstable slopes, (2) liquefaction of silts and sands, and (3) collapse of sensitive silts and clays. The second and third types are primarily limited to the Bootlegger Cove Formation, which underlies much of Anchorage. Technical studies in the years immediately following the 1964 earthquake gave support to both of these mechanisms (for example, Shannon and Wilson, Inc., 1964; Kerr and Drew, 1965; Hansen, 1965; Seed and Wilson, 1967). However, recent research has firmly demonstrated that liquefaction of sands within the formation was not the primary cause of ground failure (Idriss and Moriwaki, 1982; Updike, 1983, 1984). Thus, interest has recently begun to focus on the cyclic stress-strain behavior of the cohesive soils of the formation although actual test data for these soils have been limited. A study of the cyclic strengths of the clay and silt was performed by Seed and Chan (1964) for the postearthquake investigations that were conducted by Shannon and Wilson, Inc., for the U.S. Army Corps of Engineers. This study utilized the then-emerging technology of cyclic testing of soils. In order to better assess the potential for further landslides during future earthquakes, it is necessary to more fully understand the cyclic stress behavior in the light of current perceptions of the formation.

## Scope

The objective of this study was to establish with greater confidence the static and dynamic characteristics of the Bootlegger Cove Formation and, if possible, to relate these characteristics to basic soil index values. To achieve this objective, a comprehensive testing program was conducted to gain knowledge on formational dynamic behavior characteristics which could be applied to

<sup>1</sup>School of Engineering and Applied Science, University of California, Los Angeles, California.

<sup>2</sup>DOWL Engineers, Inc., Anchorage, Alaska.



**Figure 1.** The Turnagain Heights landslide was one of several Anchorage landslides resultant from failure of the Bootlegger Cove Formation during the 1964 Prince William Sound earthquake (Photo from NOAA/EDS files, No. 140-2).

the formation on a regional scale. During the geotechnical foundation studies for a high-rise building in downtown Anchorage, high-quality, undisturbed, thin-walled Shelby-tube samples were acquired and were provided to the authors by the building owners, with the agreement that site location would remain confidential. The testing of those samples is the focus of this report, with primary emphasis on soils typical of the Bootlegger Cove Formation in downtown Anchorage. Samples that were found to be metastable and that, in some cases, began to deform immediately after extrusion from samplers were not included in this study because of the potential problems of disturbance during transportation, extrusion, and laboratory preparation. The intent of this study is to establish a benchmark of cyclic test data on “typical” cohesive soil samples of the Bootlegger Cove Formation, from which point future studies can focus on the metastable soil horizons that are critical to future seismic stability evaluations.

## Acknowledgments

This project was supported by a grant from the Federal Emergency Management Agency (FEMA) to the Alaska Division of Emergency Services (ADES), which contracted the authors to conduct the research. The project was further supported by a cooperative agreement between the U.S. Geological Survey (USGS) and the Alaska Division of Geological and Geophysical Surveys (ADGGS) under the Earthquake Hazards Reduction Program. The testing was conducted at the geotechnical laboratories of DOWL Engineers, Anchorage; University

of California-Los Angeles Civil Engineering Department; and ADGGS Engineering Geology Section. Catherine Ulery, Peter Glaesman, and Michael Pritchard (ADGGS) assisted with the cartography. Rodney Combellick (ADGGS), Harold Olsen (USGS), Henry Schmoll (USGS), and Hans Pulpan (University of Alaska—Fairbanks Geophysical Institute) provided technical reviews of the manuscript. The owner and developer of the site where the samples were obtained has reserved the right to remain unnamed, but the drilling and field logistics support provided by that party made the project possible within the budget provided by FEMA-ADES and by USGS-ADGGS. The authors particularly wish to thank Alvaro Espinosa, (USGS, Golden, Colo.) who, through his USGS-funded Anchorage Earthquake Hazards Project, provided both the encouragement and organizational support necessary for the publication of this report.

## REGIONAL GEOLOGIC HISTORY

The Anchorage area is located in the upper Cook Inlet region of south-central Alaska. This inlet has had a varied history during Quaternary time in response to fluctuations in sea level, advance and retreat of adjacent mountain glaciers, and tectonic uplift and subsidence. The geologic record produced by the interplay of these systems is indeed complex and not well understood; however, some generalizations can be made.

## Tectonic Setting

Cook Inlet is situated in a tectonic forearc basin that is bounded to the west by the Bruin Bay-Castle Mountain fault system and to the east by the Border Ranges fault system (which includes the Knik fault along the west front of the Chugach Mountains) (fig. 2). Most of the regional seismicity can be attributed to underthrusting along the Benioff Zone of the plate boundary megathrust which extends beneath the inlet (Fogelman and others, 1978). There is, however, some evidence suggesting that both the Castle Mountain (Bruhn, 1979; Lahr and others, 1986) and Border Ranges fault systems (Updike and Ulery, 1983) may be active and capable of propagating moderate earthquakes. Each year earthquakes with magnitudes above 4.5 are felt in Anchorage as a result of this seismic setting.

The tectonic basin is bounded to the east in the Chugach Mountains by Mesozoic metamorphic rocks (graywackes, phyllites, metavolcanics, and argillites of the Valdez and McHugh Groups). To the west, the basin is confined by the igneous and metasedimentary rocks of the Alaska Range. Within the basin, and lying a few

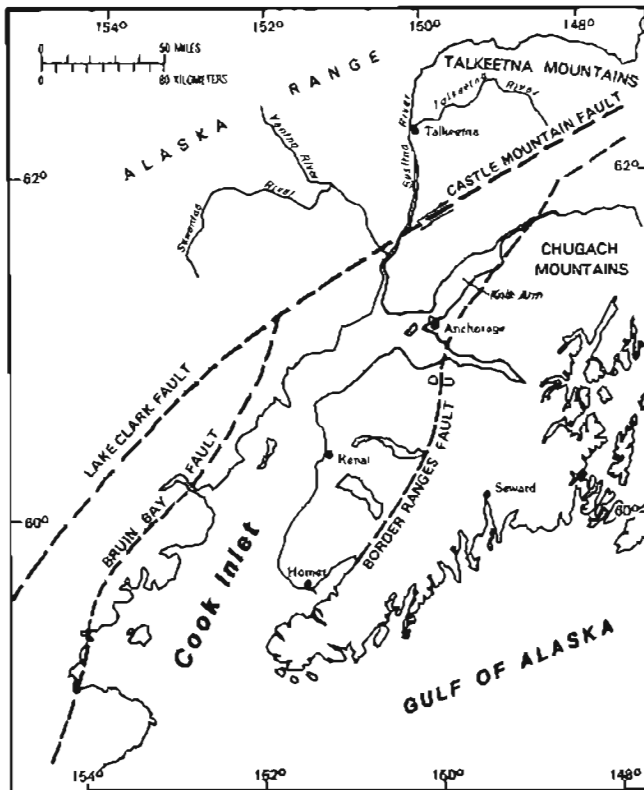


Figure 2. Generalized map showing major faults in the vicinity of Anchorage.

hundred meters below Anchorage, are Tertiary clastic sedimentary rocks that have been deposited in the structural depression; these sedimentary rocks wedge out against the older rocks along the basin boundaries.

### Quaternary History

The Quaternary history of upper Cook Inlet has been discussed in considerable detail by Miller and Dobrovolny (1959), Karlstrom (1964), Schmoll and Dobrovolny (1972), and Reger and Updike (1983). Karlstrom proposed that at least five major glaciations occurred in upper Cook Inlet which were, from oldest to youngest, Mount Susitna, Caribou Hills, Eklutna, Knik, and Naptowne glaciations. The three earlier glaciations (Mount Susitna, Caribou Hills, and Eklutna) were presumably far more extensive than the later ones (Knik and Naptowne), and ice of these earlier glaciations coalesced to fill the Cook Inlet trough. The later glaciations, though not as extensive, were capable of significantly restricting the movement of fresh and marine waters in the inlet. It is quite probable that glacially dammed lakes were produced during the late Pleistocene so that glaciofluvial, deltaic, lacustrine, and marine sedimentation were juxtaposed with ice-contact deposits.

The Bootlegger Cove Formation<sup>3</sup> was a product of this type of glaciomarine/glaciolacustrine environment. Although the following discussion relates to this stratigraphic unit as exposed in the Anchorage area, the depositional environment was undoubtedly duplicated elsewhere in Cook Inlet at various times during the Quaternary, which resulted in several other Bootlegger Cove-type deposits.

The Bootlegger Cove Formation is a stratified sequence of clastic sediments that range from clay to boulders which, on the basis of paleontologic evidence (Schmidt, 1963), were deposited in brackish or marine waters. The formation is known to occur at shallow depths beneath most of the western half of metropolitan Anchorage, as well as northward in the Knik Arm area and westward to the Susitna River. Several radiometric dates have consistently yielded a late Wisconsin age (about 14,000 years B.P.) for a horizon in the upper part of the formation (Schmoll and others, 1972). Generally, the formation is underlain by glaciofluvial sands and gravel or by glacial till. Dependant upon the location, the formation may be overlain by till (for example, the Elmendorf Moraine), glaciofluvial sediments, or eolian silts and peat.

### Engineering Geologic Facies of the Bootlegger Cove Formation

Seven sedimentary facies of the Bootlegger Cove Formation have been identified by Updike and Carpenter (1986) in order to better characterize intraformational variations of composition and geotechnical characteristics. Each facies is distinguishable as a function of subtle differences in depositional environment (for example, turbidity, energy regime) and postdepositional modifications (for example, overburden pressures, ground-water leaching). The defined facies are intricately intercalated so that the scale of units portrayed can vary depending on the objective of the study. For mapping purposes, units less than 1 m in thickness must be considered as lenses or layers within a larger facies unit (Updike, 1986; Updike and Carpenter, 1986). By contrast, a laboratory geotechnical study of the facies, such as the present report, must isolate a finite suite of undisturbed samples representative of those defined facies. The facies which have been differentiated as distinct units at both scales are:

<sup>3</sup>This stratigraphic unit was originally named the Bootlegger Cove Clay by Miller and Dobrovolny (1959) for typical sections exposed at Bootlegger Cove in Anchorage. Because the unit varies greatly in composition and because clay is commonly a secondary constituent, Updike and others (1982) have renamed the unit the Bootlegger Cove Formation.

- (3) A series of ten stress-controlled cyclic triaxial tests were conducted on intact specimens, which were initially consolidated at overconsolidation stress ratios of 1.0, 1.5, and 2.0 and tested at the appropriate cyclic stress ratios, to establish the dynamic shear moduli, damping ratios, and number of cycles to cause various amounts of strain.
- (4) A series of ten stress-controlled cyclic triaxial tests on remolded specimens of item 3, which were initially consolidated at overconsolidation stress ratios of 1.0, 1.5, and 2.0, were conducted at appropriate cyclic stress ratios to establish the dynamic shear moduli, damping ratios, and number of cycles to cause various amounts of strain.

## Unconsolidated-Undrained Tests

### Equipment

The testing equipment used for the UU tests is shown in figure 7. It consists of a triaxial cell placed in a 5-ton Wykeham Farrance<sup>4</sup> loading machine. A confining pressure is applied in the triaxial cell by air pressure, which is regulated and measured as shown on the left side of figure 7. A load cell, mounted below the cross bar on the loading machine, is used to measure the vertical deviator load that is applied to the triaxial specimen. The electrical signal from the load cell is measured by the BLH Strain Indicator shown on the right side of figure 7. A dial gauge is employed to measure the vertical deformation of the specimen.

### Testing Procedure

The intact soil was trimmed to produce a final cylindrical specimen with a diameter of 1.40 inches (3.57 cm) and a height of 3.00–3.50 inches (7.62–8.89 cm) for UU testing. The specimen was inspected, and a sketch with location and geometry of sedimentary laminae was drawn. The specimen was measured and weighed for determination of wet density. The specimen was then placed between a lucite cap and base, and two rubber membranes, each 0.002 inches (0.005 cm) thick, were rolled up around it. A layer of high-vacuum silicone grease was smeared on the inner membrane before the outer membrane was rolled up. Two O-rings were used



Figure 7. Triaxial testing equipment used for the unconsolidated-undrained static tests.

on each end to seal the membranes to the cap and base. The specimen was then placed in the triaxial cell, and a confining pressure of 50 psi (3.52 kg/cm<sup>2</sup>) was applied by compressed air. The specimen was sheared at a constant rate of deformation of 0.020 inches/minute (0.050 cm/minute), which corresponds to a strain rate of 0.57 percent/minute for a 3.50-inch (8.89 cm) specimen and 0.67 percent/minute for a 3.00-inch (7.62 cm) specimen. Measurements of load and deformation were taken at appropriate intervals throughout the test. At the end of each test, the triaxial cell was disassembled and the membranes were carefully removed to inspect the final shape of the specimen, to locate shear planes (recorded on a sketch), and to take a photograph of the failed specimen.

To perform a UU test on remolded soil, the previously intact specimen was mixed with part of the rough trimmings and thoroughly remolded. A cylindrical specimen was trimmed from the remolded soil, measured and weighed, and placed between the cap and base. The remolded specimen was tested under UU conditions without membranes and without confining pressure. The testing procedure for the remolded specimen was otherwise similar to that described above for the intact specimen.

<sup>4</sup>Any use of trade names in this report is for descriptive purposes only and does not imply endorsement by the U.S. Geological Survey.

In addition to the ten UU tests on remolded soil performed without confining pressure, for comparative purposes, one UU test on remolded soil was performed on sample CT-8 (F.II) with a confining pressure of 50 psi (3.52 kg/cm<sup>2</sup>). For this specimen the membranes were mounted around the soft remolded specimen using a vacuum jacket.

## Consolidated-Undrained Tests

### Equipment

The testing equipment used for consolidated-undrained (CU) tests is shown in figure 8. It consists of a triaxial cell placed in a 5-ton Wykeham Farrance loading machine. The cell water is pressurized by regulated air pressure in a separate lucite cylinder connected with the cell. This arrangement is used to avoid air penetration through the specimen membranes, thereby maintaining a high degree of saturation of the specimen. The drainage line from the triaxial specimen is connected to a volume change and pore pressure measuring device shown at the right in figure 8. A back pressure can be applied in the specimen through this device. A load cell, mounted below the cross bar on the loading machine, is used to measure the vertical deviator load applied to the specimen. An LVDT (linear variable displacement transducer) is employed to measure the vertical deformation of the specimen. The electrical signals from the load cell, the pore pressure transducer, and the LVDT were measured and recorded by the Digitec 1000 datalogger shown at the left in figure 8.

### Testing Procedure

The CU tests were performed only on remolded specimens because the limited intact sample material that was available needed to be conserved for the dynamic tests. The remolded specimen previously tested under UU conditions was again mixed with part of the rough trimmings and thoroughly remolded. A cylindrical specimen with a diameter of 1.40 inches (3.57 cm) and a height of 3.00–3.50 inches (7.62–8.89 cm) was trimmed from the remolded soil, measured, and weighed. A water-saturated carborundum filter stone was fitted on the stainless steel base to provide drainage for the CU specimen, which was placed on the filter stone. A lucite cap was placed directly on top of the specimen. Vertically slotted filter paper was wrapped around the specimen to provide radial drainage. The filter paper was then wetted to make it cling to the specimen. The O-ring at the end of the inner rubber

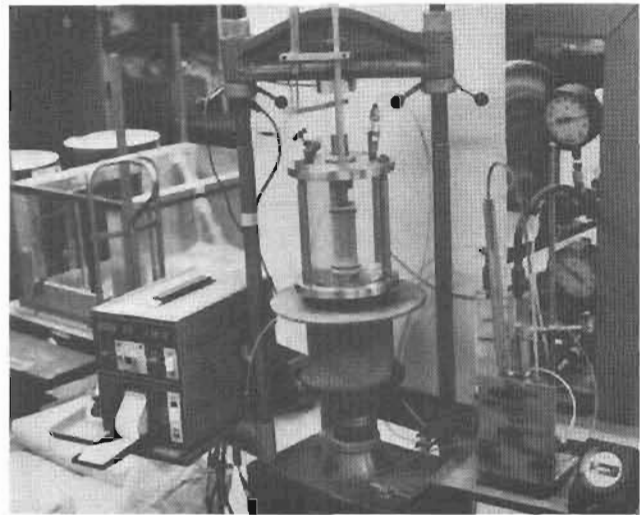


Figure 8. Triaxial testing equipment used for the isotropically consolidated-undrained static tests.

membrane was cut off to avoid penetration into the soft remolded soil. Without this O-ring and with the additional strength provided by the filter paper drains, it was possible to roll the inner membrane up around the specimen, while avoiding severe indentation in the specimen. A thin layer of high-vacuum silicone grease was smeared on the inner membrane before the outer membrane was rolled up. Two O-rings were used on each end to seal the membranes to the cap and base. After having assembled the specimen on the bottom plate of the triaxial cell, the cell wall and the top plate were installed, the cell was filled with de-aired water, and a confining pressure was applied.

With the drainage line connected to the volume change and pore pressure measuring device and with the drainage valve closed, the desired cell pressure of 80 psi (5.63 kg/cm<sup>2</sup>) and back pressure of 30 psi (2.11 kg/cm<sup>2</sup>) were applied. An effective isotropic confining pressure (cell pressure minus back pressure) of 50 psi (3.52 kg/cm<sup>2</sup>) was employed in all tests. By opening the drainage valve, the specimen was allowed to consolidate isotropically; in other words, it was an isotropically consolidated-undrained (ICU) test. Measurements of volume change, vertical deformation, and time were taken to produce a consolidation-time curve. The information from this curve was used to calculate an allowable vertical strain rate for the undrained shearing of the specimen. Because a datalogger was employed for the shearing phase of the test, it was possible to further reduce the vertical strain rate, thus insuring a high degree of pore water pressure equalization inside the specimen. A deformation rate of 0.00024 inches/minute (0.0006 cm/minute) was used in all tests except those on samples CT-1 (0.00016 inches/minute; 0.0004 cm/minute) and CT-6 (0.00048 inches/minute; 0.0012 cm/minute).

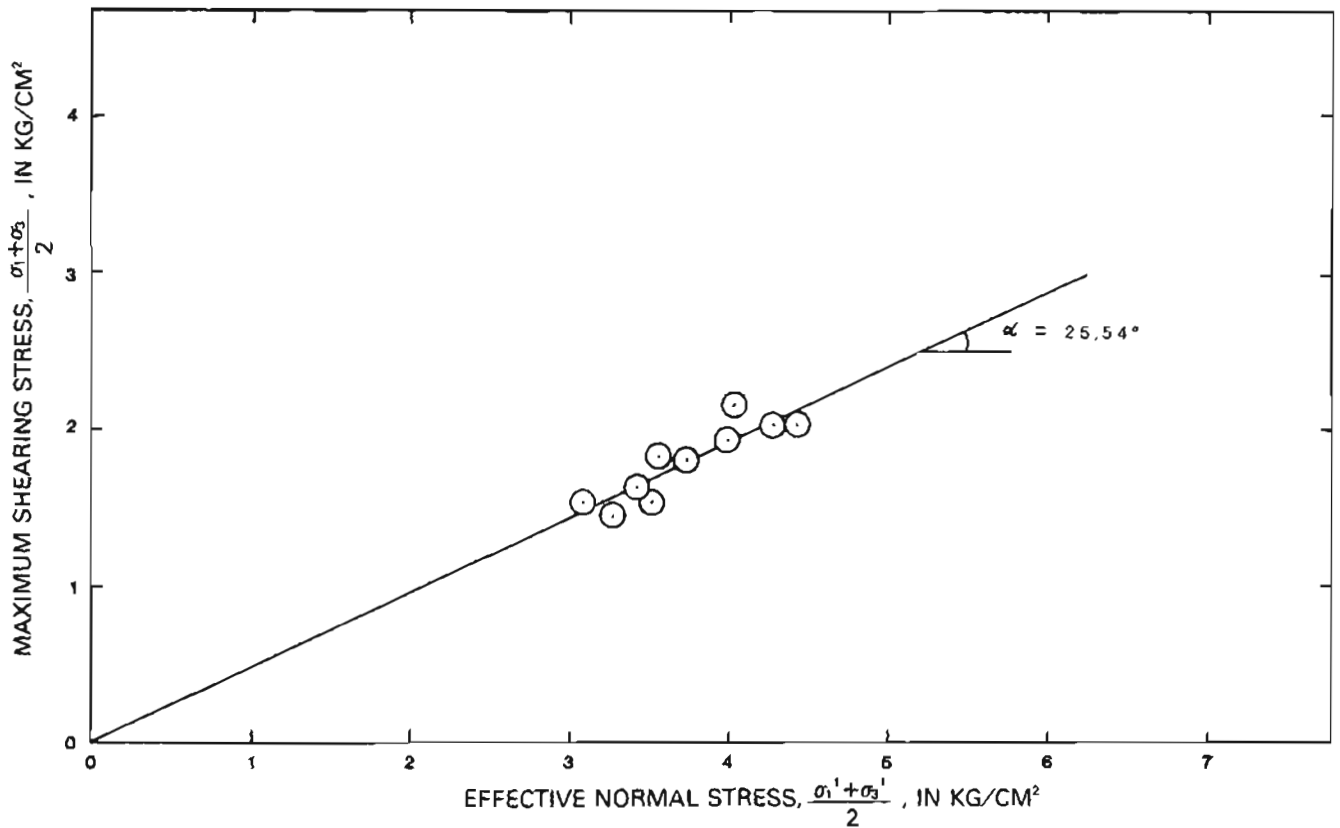


Figure 12. The p-q diagram of effective normal stress versus maximum shearing stress as determined by ten isotropically consolidated-undrained tests on the Bootlegger Cove Formation. The angle of inclination,  $\alpha$ , of the "best-fit line",  $K_p$ , through the points is  $25.54^\circ$ .

### Cyclic Loading Tests

The initial conditions and the stress conditions for the cyclic loading tests on intact specimens are summarized in table 4, and those for the cyclic loading tests on remolded specimens are summarized in table 5. These tables contain the water contents, specimen geometries, initial wet densities, vertical and volumetric strains due to consolidation, consolidation times, coefficients of consolidation, actual  $K_c$ -values, and stresses applied during static and cyclic phases of the tests. These tables also show that the  $B$ -values for the triaxial specimens decrease with increasing consolidation stress ratios. This behavior does correspond to fully saturated specimens as discussed in detail by Lade and Kirkgard (1984). Detailed test results including sketches of intact specimens, consolidation curves, and X-Y recordings of cyclic stress-strain relationships were also recorded. Figures 13-15 show representative deformed shapes of three samples, under both intact and remolded initial conditions.

### Strength Relations for Intact Specimens

In order to interpret the strength results of the

cyclic loading tests that were performed on specimens with consolidation ratios of  $K_c = 1.0$ , the axial peak-to-peak strains are plotted versus number of cycles on a semilog diagram for different cyclic stress ratios (fig. 16). The cyclic stress ratio is defined as  $\sigma_{dmax}/2S_u$ , in which  $S_u$  is the static undrained strength and  $\sigma_{dmax} = \sigma_{dc} + \sigma_{dp}$ , in which  $\sigma_{dc}$  is the stress difference during consolidation and  $\sigma_{dp}$  is the cyclic (pulsating) stress difference. Based on the diagram in figure 16, another diagram is constructed in which the cyclic stress ratio is plotted versus the number of cycles that are required to cause various amounts of axial peak-to-peak strains (figs. 17, 18).

The values of undrained shear strength,  $S_u$ , that were determined from the UU tests on intact specimens were used for calculation of the cyclic stress ratio shown in figure 17. ICU tests on intact specimens were not performed. However, based on the shear strength diagram in figure 11, approximate values of  $S_u$  from tests on intact specimens were estimated and used for the cyclic stress ratios employed in figure 18. Diagrams of this type are plotted for all cyclic tests on intact specimens. These diagrams are produced to make a direct comparison of results from cyclic loading tests on intact and remolded

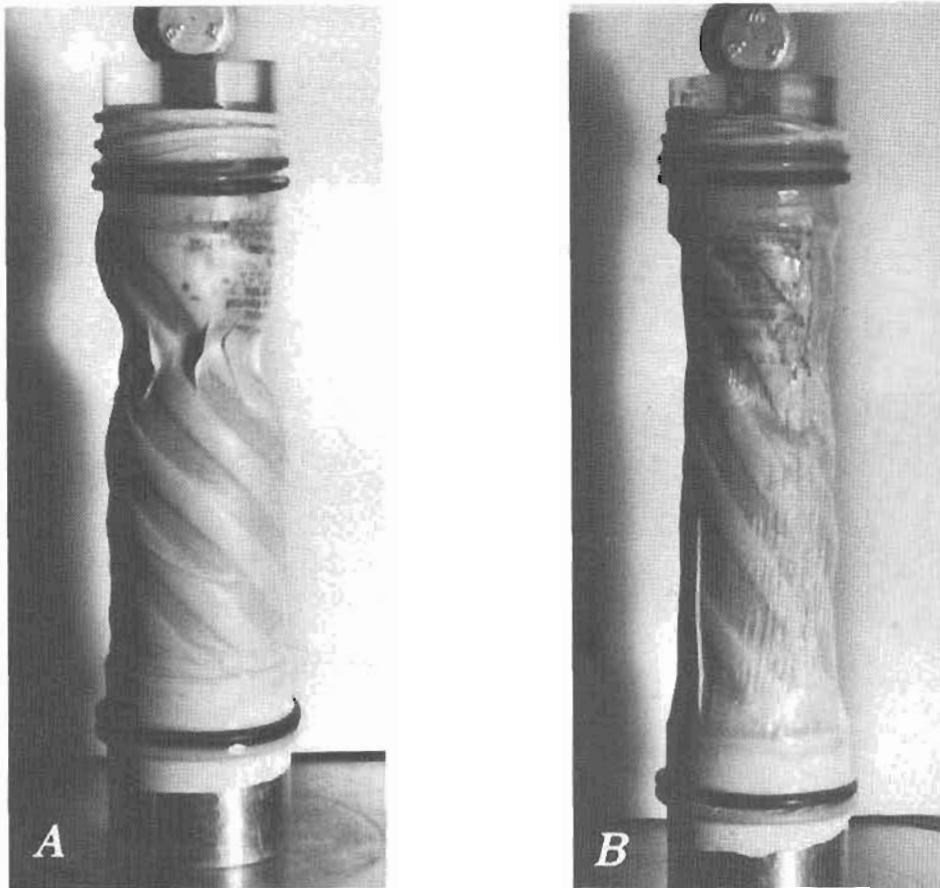


Figure 13. Specimen CT-5 (facies F.IV of the Bootlegger Cove Formation) after consolidation at stress ratio,  $K_c = 1.0$ , and after failure by cyclic loading. Note the sample failed in extension. A, Intact specimen; B, Remolded specimen. Specimen about 15 cm long.

specimens. For this comparison a common basis, such as results of ICU tests, is required.

There are, however, several reasons why the estimated values of undrained shear strength from ICU tests on intact specimens may be incorrect. The estimated strengths are based on results from tests on remolded specimens or from tests on intact specimens which were first exposed to resonant column testing (see fig. 11). Because remolded or disturbed specimens may behave differently from intact specimens of sensitive soils, it is preferable to employ truly intact specimens for determination of undrained shear strengths. Therefore, to provide a common basis for comparisons of the type described above, ICU tests on intact specimens should be performed in connection with future studies of the cyclic behavior of the Bootlegger Cove Formation. Unfortunately, this work was beyond the scope of funding and sample availability in the present study.

For the cyclic loading tests with initial consolidation stress ratios of  $K_c = 1.5$  and 2.0, the maximum axial strains are plotted versus number of cycles on

semilog diagrams for different cyclic stress ratios for intact specimens (figs. 19, 20). Based on these diagrams, other diagrams are constructed on which the cyclic stress ratio is plotted versus the number of cycles that are required to cause various amounts of maximum axial strains (figs. 21-24).

The permanent axial strains observed in the cyclic loading tests on specimens with  $K_c = 1.0$  are negative and relatively small, and this corresponds to failure in extension as observed in these tests (see fig. 13). The permanent axial strains obtained in tests with  $K_c = 1.5$  and 2.0 are positive and increase to large values, and failure in these tests occurs in compression (figs. 14, 15). The axial peak-to-peak strains in these tests are comparatively small ( $\epsilon_{max} = 3$  percent for  $K_c = 1.5$ , and  $\epsilon_{max} = 0.4$  percent for  $K_c = 2.0$ ). Thus, a common basis for a direct comparison between tests with  $K_c = 1.0$  and tests with  $K_c = 1.5$  and 2.0 is absent. Nevertheless, to get an idea of the relative strengths obtained from the tests with different  $K_c$ -values, cyclic stress ratios are plotted versus number of cycles on a semilog diagram for axial

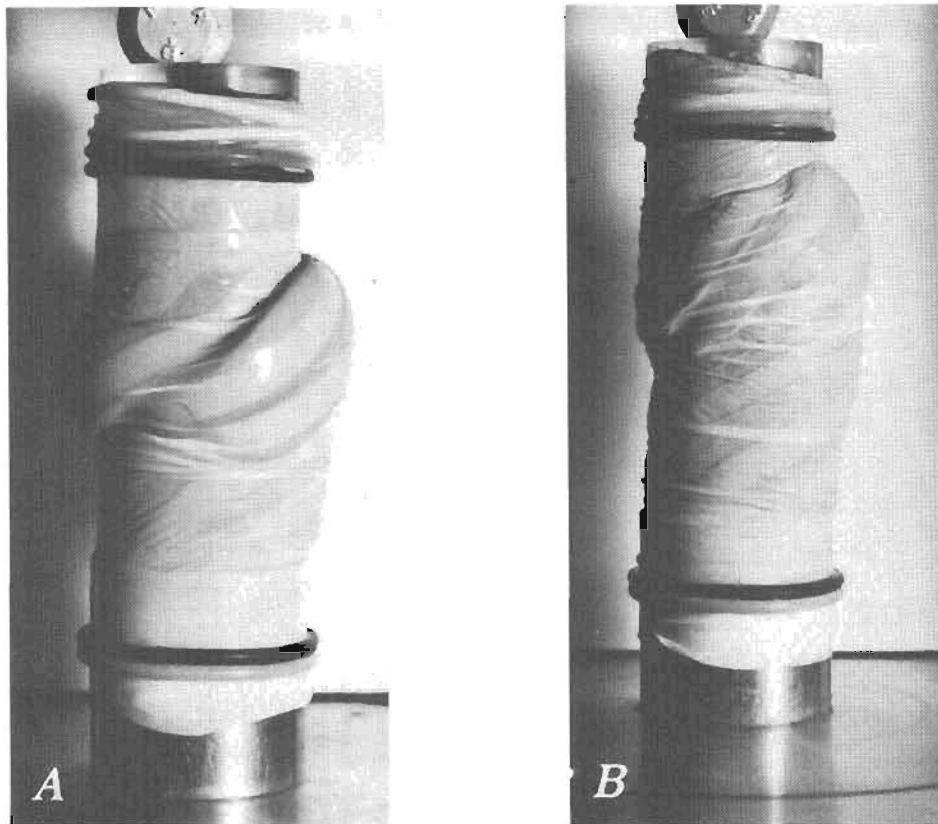


**Figure 14.** Specimen CT-3 (facies F.III of the Bootlegger Cove Formation) after consolidation at stress ratio,  $K_c = 1.5$ , and after failure by cyclic loading. Note the sample failed in compression. *A*, Intact specimen; *B*, Remolded specimen. Specimen about 15 cm long.

peak-to-peak strains of 5.0 for  $K_c = 1.0$  and for maximum axial strains of 10 percent for  $K_c = 1.5$  and 2.0 (fig. 25). This figure indicates that the cyclic stress ratio to cause 10 percent axial strain (peak-to-peak or maximum) increases with increasing consolidation stress ratio for a given number of cycles.

### Discussion of Cyclic Stress Ratio

The cyclic stress ratios discussed above involve the undrained shear strengths that were determined from the UU tests on intact specimens. In an attempt to obtain a direct comparison between tests on intact soil and tests on remolded soil, the cyclic load applied in the tests on intact specimens was also used for the remolded specimens. Thus, it was not necessary to rely on a static undrained shear strength for the remolded soil to estimate the cyclic stress from a cyclic stress ratio. However, due to the larger amounts of volume change for the remolded specimens, the cross-sectional areas of these specimens were smaller and the cyclic stress therefore was higher for the remolded specimens than for the intact specimens.

Depending upon the objective, it is possible to use two different static, undrained shear strengths for calculation of the cyclic stress ratio for remolded soil: (1) that obtained from UU tests, and (2) that obtained from ICU tests. The first value is very easy to obtain, but it is a small number with substantial scatter, which results in high cyclic load ratios with significant scatter. Furthermore, this value does not reflect the consolidation that follows disturbance due to an earthquake. To obtain the second value requires relatively advanced equipment and a considerable amount of time. However, the second value is much higher and should be more consistent than the first value. Its use will result in lower cyclic stress ratios, with less scatter. Both values have been employed in separate evaluations of the cyclic loading tests on remolded soil.

### Strength Relations for Remolded Specimens

The procedure for evaluation of the cyclic loading tests on remolded specimens is similar to that described above for the intact specimens. Figures 26–28 show the

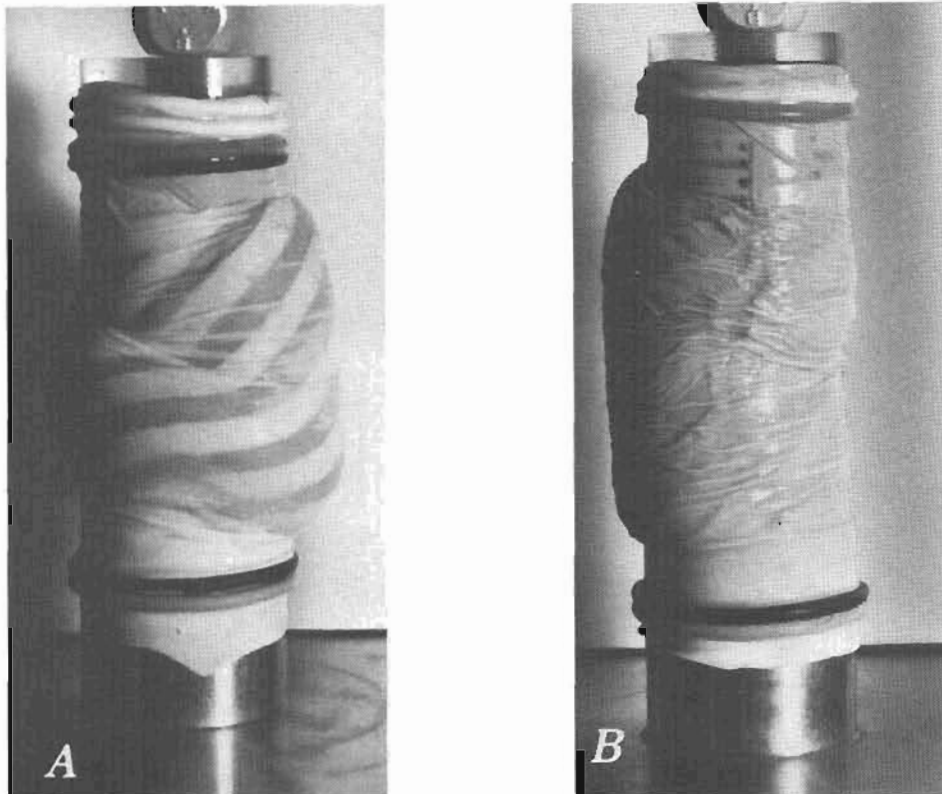


**Figure 15.** Specimen CT-4 (facies F.IV of the Bootlegger Cove Formation) after consolidation at stress ratio,  $K_c = 2.0$ , and after failure by cyclic loading. Note the sample failed by compression. A, Intact specimen; B, Remolded specimen. Specimen about 15 cm long.

axial strains (peak-to-peak for  $K_c = 1.0$  and maximum for  $K_c = 1.5$  and 2.0) plotted versus number of cycles for tests with various cyclic stress ratios. Corresponding to the two different types of undrained shear strengths, two values of cyclic stress ratios are indicated on these figures. Figures 29-31 show the cyclic stress ratios in terms of the undrained shear strength from the UU tests plotted versus the number of cycles that are required to cause various amounts of axial strain. In figures 32-34, the cyclic stress ratios in terms of the undrained shear strength from the ICU tests are plotted versus the number of cycles that are required to cause various amounts of axial strain. The application of the strengths from the UU tests results in much higher stress ratios than those obtained using the strengths from the ICU tests.

### Comparison of Strength Relations for Intact and Remolded Specimens

Using the undrained shear strength from the UU tests, a comparison of all tests on remolded soils is shown in figure 35. Despite the problems with such a comparison, it can be seen that the cyclic stress ratio that is

required to cause 10 percent axial strains (peak-to-peak or maximum) increases with increasing consolidation stress ratio for a given number of cycles. The test results for the intact specimens are also shown on figure 35, and the cyclic stress ratios that are required to cause 10 percent axial strain in these specimens are much smaller than those required for the remolded specimens. It should be recalled, however, that the unconfined shear strength used for the remolded soil does not reflect the effect of consolidation after remolding. These strengths are relatively small and result in high cyclic stress ratios for the remolded specimens.

Using the undrained shear strength from the ICU tests, a comparison of all tests on remolded soil is shown in figure 36. The cyclic stress ratios are substantially lower than those shown in figure 35, but the conclusions regarding the cyclic strength are similar to those presented above. In comparing the cyclic stress ratios for the remolded specimens with those for intact specimens (fig. 37), it appears that the intact specimens are stronger than the remolded specimens. However, this is misleading. The undrained shear strengths used in the cyclic stress ratios are not directly comparable because the intact specimens are exposed to lower effective confining pressures in the

**Table 4. Summary of initial and stress conditions for cyclic loading tests on Bootlegger Cove Formation intact specimens**  
 [See "GLOSSARY OF SYMBOLS USED" for definitions of symbols]

Sample	CT-1	CT-2	CT-3	CT-4	CT-5	CT-6	CT-7	CT-8	CT-9	RC-6
<b>Before consolidation</b>										
w/c (trimmings)(%)	28.06	30.08	38.47	32.68	30.66	28.65	23.13	34.40	31.69	29.76
A <sub>o</sub> (cm <sup>2</sup> )	9.931	9.931	9.931	9.931	9.931	9.931	9.931	9.931	9.931	9.931
H <sub>o</sub> (cm)	7.518	8.839	8.433	8.585	8.484	8.407	8.814	8.814	7.087	8.839
V <sub>o</sub> (cm <sup>3</sup> )	74.67	87.78	83.75	85.26	84.25	83.49	87.53	87.53	70.38	87.78
γ <sub>wet</sub> (g/cm <sup>3</sup> )	1.981	1.983	1.865	1.944	1.957	2.000	2.079	1.935	1.957	1.980
<b>After consolidation</b>										
ΔV <sub>conso1</sub> (cm <sup>3</sup> )	5.587	6.315	5.686	7.691	4.599	4.230	2.674	5.188	4.100	5.467
Δδ <sub>conso1</sub> (cm)	0.219	0.401	0.562	1.189	0.249	0.264	0.280	0.353	0.456	0.221
ε <sub>v</sub> conso1 (%)	7.48/	7.19/	6.79/	9.02/	5.46/	5.07/	3.05/	5.93/	5.83/	6.23/
ε <sub>l</sub> conso1 (%)	2.91	4.54	6.67	13.84	2.94	3.14	3.18	4.01	6.43	2.50
A <sub>c</sub> (cm <sup>2</sup> )	9.464	9.66	9.92	10.49	9.67	9.73	9.94	9.73	10.00	9.55
H <sub>c</sub> (cm)	7.30	8.39	7.87	7.40	8.23	8.15	8.53	8.46	6.63	8.62
t <sub>50</sub> (min)	14	150	56	70	86	32	100	70	92	
t <sub>100</sub> (min)	94	760	270	440	420	150	740	500	430	
σ <sub>3c</sub> (kg/cm <sup>2</sup> )	3.515	3.515	3.515	3.515	3.515	3.515	3.515	3.515	3.515	3.515
σ <sub>dc</sub> (kg/cm <sup>2</sup> ) <sup>1</sup>	0.0	1.807	1.759	3.328	0.0	0.0	3.512	1.794	3.491	0.0
K <sub>c</sub> = σ <sub>1c</sub> /σ <sub>3c</sub>	1.0	1.514	1.501	1.947	1.0	1.0	1.999	1.510	1.993	1.0
c <sub>v</sub> ·10 <sup>5</sup> (cm <sup>2</sup> /sec)	11.823	1.261	1.455	3.378	2.702	2.200	5.911	1.892	0.370	2.056
B-value <sup>2</sup>	1.012	0.938/	0.890	0.878	1.028/	0.967	0.769	0.983/	0.935/	0.929/
		1.012						0.894/	0.884/	1.000
								0.882		
K <sub>c</sub> /Delay (min)	1.0/10	1.5/5,	1.5/5	2.0/5	1.0/5	1.0/5	2.0/5	1.0/5,	1.0/5,	1.0/5,
		1.5/10						1.5/5,	1.5/5,	1.0/10
								2.0/5		
<b>Cyclic Loading</b>										
Frequency (Hz)	1	1	1	1	1	1	1	1	1	1
#P <sub>dp</sub> (kg)	±14.9	±20.8	±16.0	±20.7	±19.6	±35.9	±22.7	±17.2	±16.5	±17.3
±σ <sub>dp</sub> = #P <sub>dp</sub> /A <sub>c</sub>	±1.58	±2.15	±1.61	±1.97	±2.03	±3.69	±2.28	±1.77	±1.65	±1.81
(kg/cm <sup>2</sup> ).										
σ <sub>dmax</sub> = σ <sub>dc</sub> + σ <sub>dp</sub>	1.58	3.96	3.37	5.30	2.03	3.69	5.79	3.56	5.14	1.81
(kg/cm <sup>2</sup> ).										
S <sub>u</sub> (static)(kg/cm <sup>2</sup> )	0.507	0.624	0.672	0.531	0.603	1.126	0.798	0.620	0.829	0.560
S <sub>p</sub> /S <sub>u</sub> (S <sub>p</sub> = 1/2σ <sub>dp</sub> )	1.56	1.72	1.20	1.86	1.68	1.164	1.43	1.43	1.00	1.62
N <sub>max</sub> [=N <sub>F</sub> ]	[=75]	[=14]	[=26]	[=47]	[=15]	[=2]	[=96]	[=31]	[=75]	[=32]
σ <sub>dmax</sub> /2S <sub>u</sub>	1.56	3.17	2.51	4.99	1.68	1.64	3.63	2.87	3.10	1.62

<sup>1</sup>g-values are determined after 5 minutes or, in a few cases, after 10 minutes.

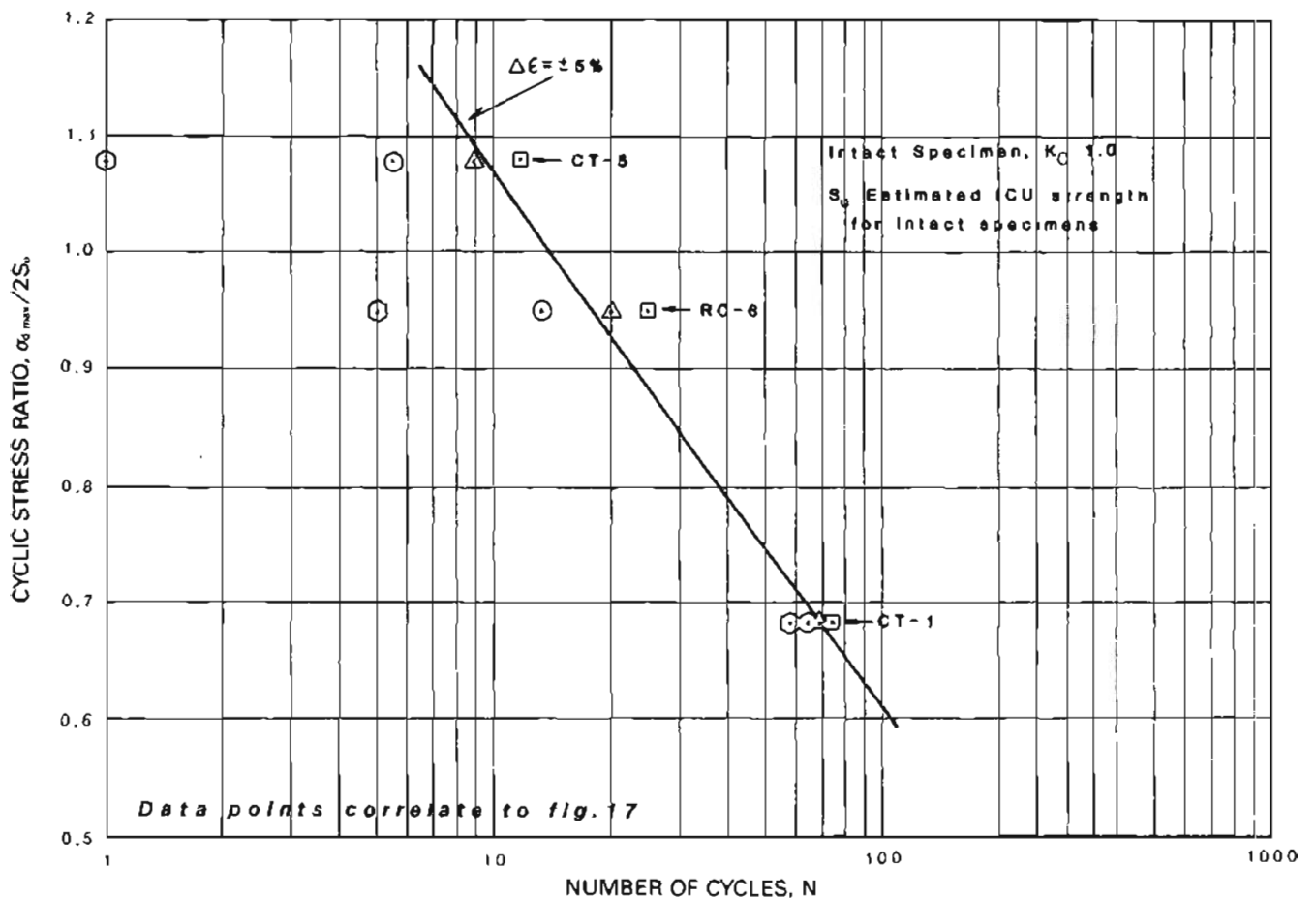


Figure 18. Cyclic stress ratio versus number of cycles for three intact specimens at initial consolidation ratio of 1.0 and using strength values estimated from isotropically undrained testing.

## SUMMARY AND CONCLUSIONS FROM LABORATORY TESTING

Ten undisturbed samples of the Bootlegger Cove Formation (mainly facies II and IV) have been tested in an investigation of representative formational stress-strain and strength properties under static and cyclic loading conditions. Soil index tests were performed in this investigation to determine liquid and plastic limits, grain-size distributions, water contents, and densities. Static undrained strength tests such as torvane and unconsolidated-undrained triaxial compression tests were performed on intact and remolded specimens, whereas isotropically consolidated-undrained tests were performed on remolded specimens. Cyclic triaxial loading tests were performed on intact and remolded specimens with initial consolidation stress ratios of 1.0, 1.5, and 2.0. The static tests were performed to serve as background and basis for evaluation of the cyclic loading tests. The latter tests were performed to establish the number of cycles and

cyclic stress ratios that are required to cause various amounts of strain, and to determine the magnitude and variation of the shear moduli and the damping ratios with single-amplitude shear strain.

The results of the cyclic loading tests indicate that higher cyclic stress ratios are required at higher consolidation stress ratios to cause a given amount of strain in a given number of cycles. Although the basis for comparison between results from intact and remolded specimens is questionable, it appears that they may have equivalent strengths. Although the data base is insufficient to provide completely conclusive statements to this effect, there is an indication that soils remolded in landslide areas have strengths equal to that of soils in areas that have not failed. This conclusion would significantly modify current concern in Anchorage for construction on old landslides.

The relationship between shear moduli and single-amplitude shear strain obtained from cyclic loading and resonant column tests shows a pattern similar to that suggested by Seed and Idriss (1970). The magnitudes of normalized shear moduli compare best with the Seed-Idriss

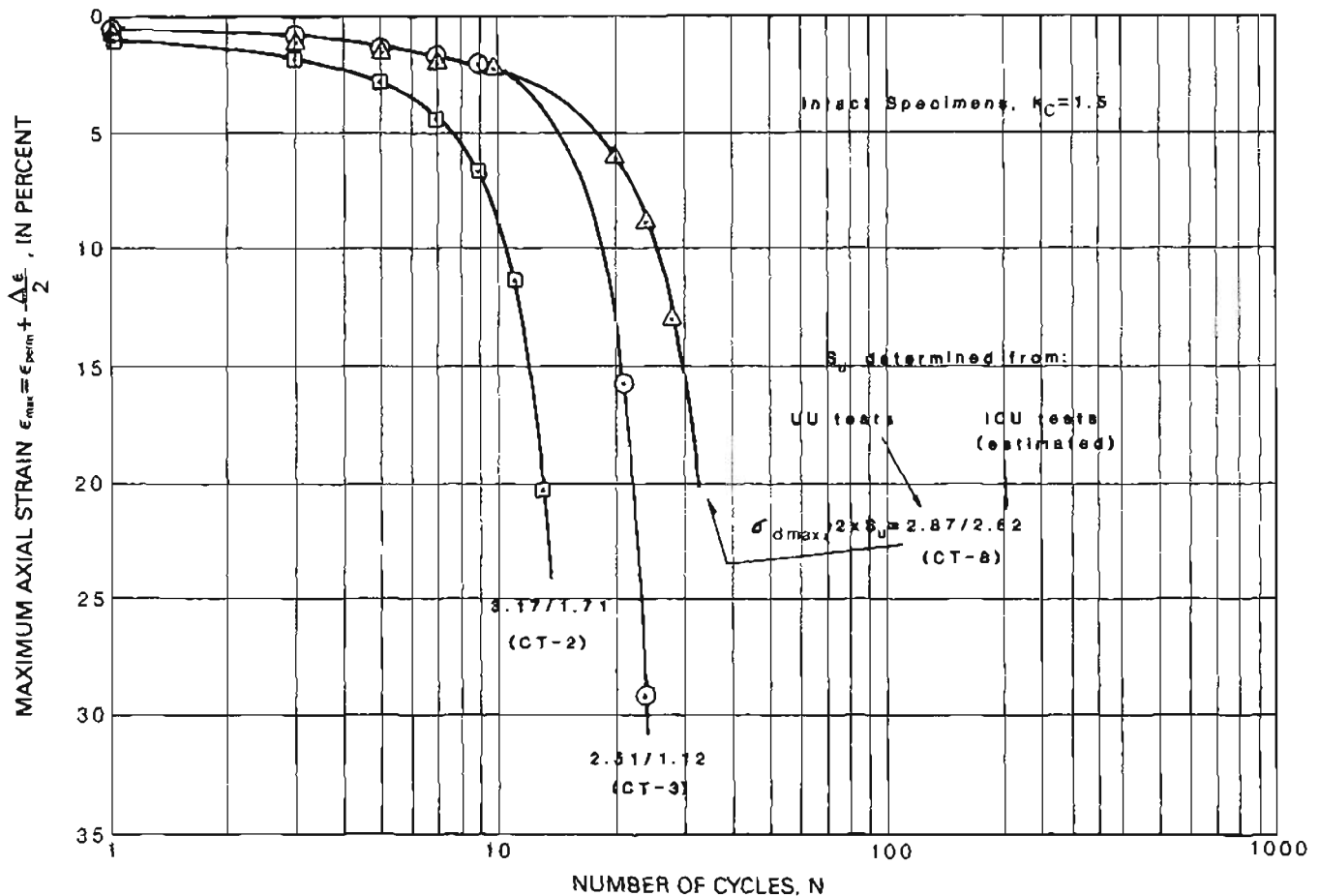


Figure 19. Maximum axial strain versus number of cycles for three intact specimens at initial consolidation stress ratios of 1.5.

values when the experimental data are normalized on the basis of shear strengths obtained from isotropically consolidated-undrained shear tests (figs. 40, 42). The damping ratios from these tests show considerable scatter but generally follow the relationship proposed by Seed and Idriss (1970).

All the samples were collected from depths between 81 and 97 ft. The sediments in this interval were deposited during the quiet-water glaciolacustrine episode of accumulation of clay and silt. It is within this stratigraphic interval that the soil failures associated with the 1964 Prince William Sound earthquake are believed to have occurred (Shannon and Wilson, Inc., 1964; Updike, 1986). It should be noted that none of the samples tested yielded sensitivity values above 12. As previously noted, concerns for sample disturbance effects manifest in the more unstable samples combined with the intent to characterize the "typical" cohesive facies of the formation dictated the range of sample types tested. Nevertheless, the sensitivity values, which are generally below 10, pose the question as to whether the Bootlegger Cove Formation can be characterized as having soil horizons of ex-

tremely high sensitivity that would fail under seismic loading. It may be shown by future testing that failure-zone soils are collapsing or liquefying under a mechanism that is as yet poorly understood. If this is the case, then the traditional approach of assessing ground failure potential of the cohesive facies of the formation based strictly on sensitivity ratios is erroneous. In light of the fact that soils within the tested interval did fail in 1964, the test data reported here must be taken as a baseline for future assessment of ground failure potential in downtown Anchorage. Strength data determined from future testing that are significantly divergent from our data may identify the soils responsible for failure.

The foregoing presentation of data and interpretation is intended to "calibrate" the static and dynamic behavior of the cohesive facies of the Bootlegger Cove Formation. In order to further enhance this insight, a companion study should conduct static ICU tests on both intact and remolded soil in order to provide a common and consistent basis for comparison of results obtained from the cyclic loading tests. The emphasis of the study reported here was to conduct a carefully monitored

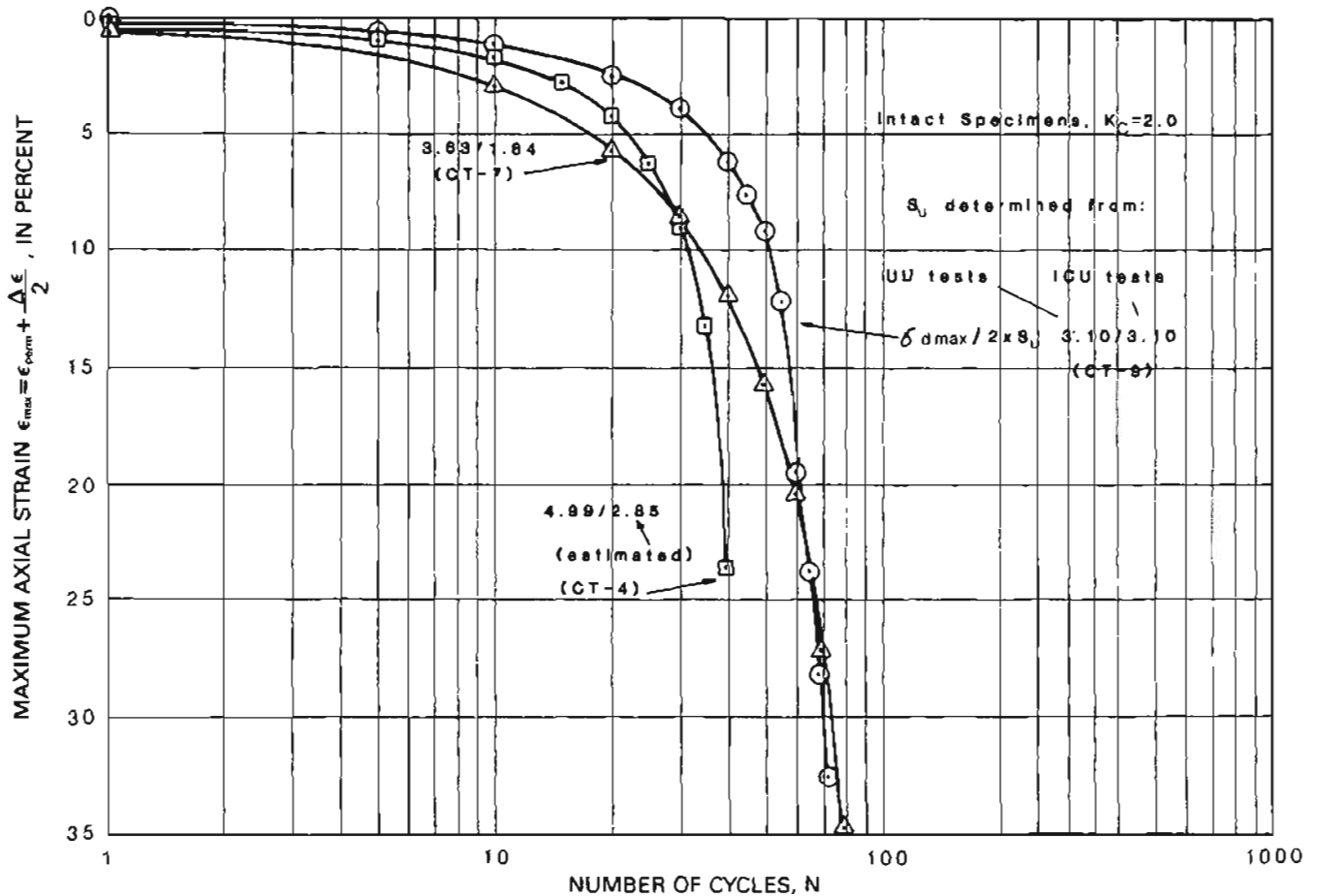
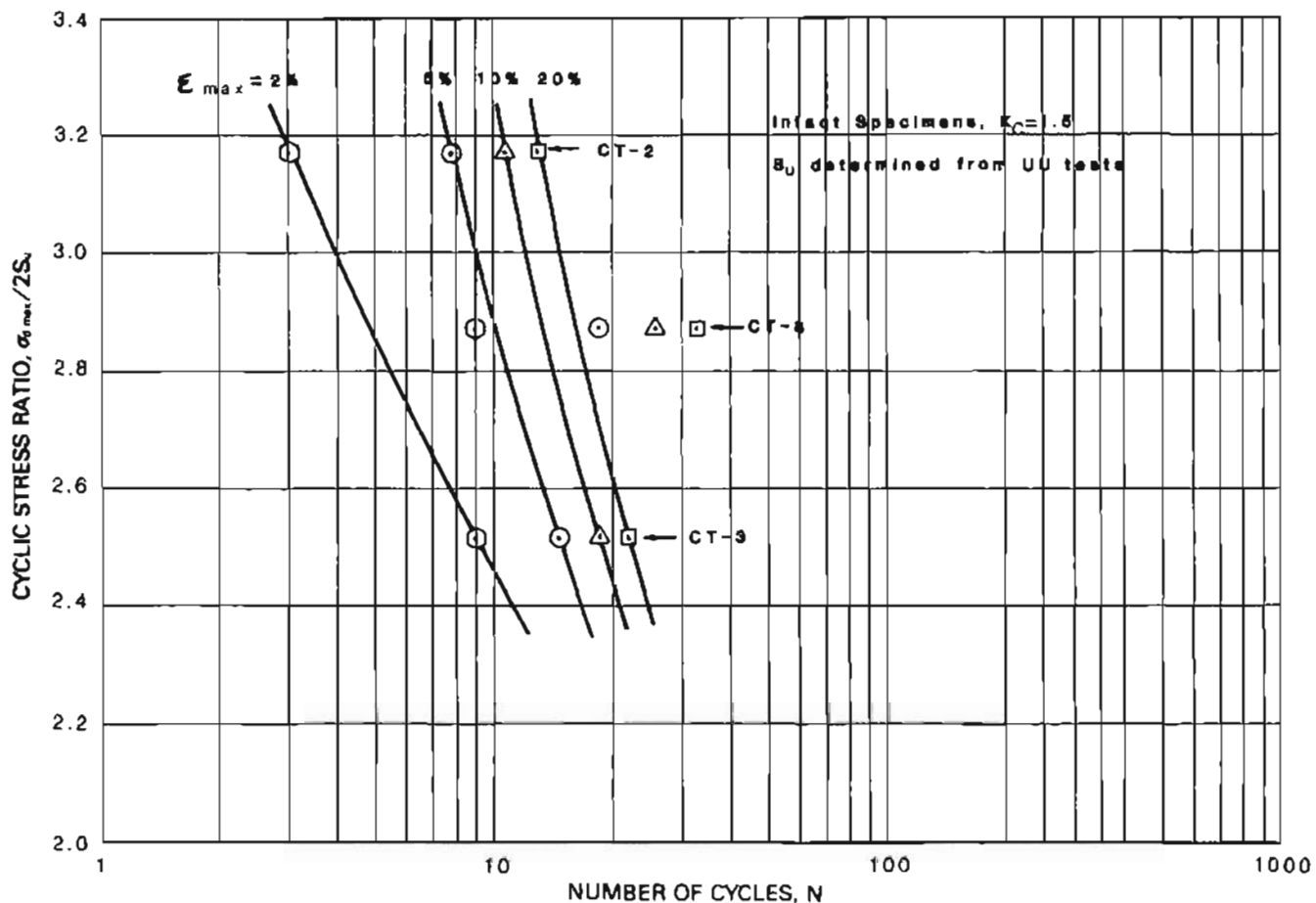


Figure 20. Maximum axial strain versus number of cycles for three intact specimens at initial consolidation stress ratios of 2.0.

sequence of static and dynamic triaxial tests on typical specimens of the Bootlegger Cove Formation. Highly sensitive specimens of facies F.III were intentionally avoided because the anticipated response of this facies would not benefit the objective of the study, which was to establish behavior norms for the predominant facies. The authors recommend that future investigations explore the comparative cyclic properties of each cohesive facies of the formation.

## REFERENCES CITED

- Bruhn, R.L., 1979, Holocene displacements measured by trenching the Castle Mountain Fault near Houston, Alaska: Alaska Division of Geological and Geophysical Surveys Geologic Report 61, p. 1-4.
- Fogelman, K., Stephens, C., Lahr, J.C., Helton, S., and Allen, M., 1978, Catalog of earthquakes in southern Alaska, October-December, 1977: U.S. Geological Survey Open-File Report 78-1097, 28 p.
- Hansen, W.R., 1965, Effects of the earthquake of March 27, 1964, at Anchorage, Alaska: U.S. Geological Survey Professional Paper 542-A, p. A1-A68.
- Idriss, I.M., and Moriwaki, Yoshihau, 1982, Anchorage Office Complex geotechnical investigation, Anchorage, Alaska, v. 1, Seismic hazards evaluation: San Francisco, Woodward-Clyde Consultants, p. 6-1 to 6-3.
- Karlstrom, T.N.V., 1964, Quaternary geology of the Kenai Lowland and glacial history of the Cook Inlet Region, Alaska: U.S. Geological Survey Professional Paper 443, 69 p.
- Kerr, P.F., and Drew, I.M., 1965, Quick clay movements, Anchorage, Alaska: Springfield, Va., National Technical Information Service, Document AD630-11, 133 p.
- Lade, P.V., and Kirkgard, M.M., 1984, B-value tests for soil specimens with anisotropic stress states: American Society of Civil Engineers, 5th Engineering Mechanics Division Specialty Conference, Laramie, Wyoming, Proceedings, p. 1304-1307.
- Lahr, J.C., Page, R.A., Stephens, C.D., and Fogleman, K.A., 1986, Sutton, Alaska, earthquake of 1984—evidence for activity on the Talkeetna segment of the Castle Mountain fault system: Seismological Society of America Bulletin, v. 76, p. 967-983.



**Figure 21.** Cyclic stress ratio (determined from unconsolidated-undrained tests) versus number of cycles, for three intact specimens under initial consolidation ratio of 1.5.

Lambe, T.W., and Whitman, R.V., 1979, Soil mechanics, SI version: New York, John Wiley, 553 p.

Miller, R.D., and Dobrovlny, E., 1959, Surficial geology of Anchorage and vicinity, Alaska: U.S. Geological Survey Bulletin 1093, 128 p.

Reger, R.D., and Updike, R.G., 1983, Upper Cook Inlet region and the Matanuska Valley, in Pewe, T.L., and Reger, R.D., Richardson and Glenn Highways—Guidebook to permafrost and Quaternary geology: Alaska Division of Geological and Geophysical Surveys Guidebook 1, p. 185-263.

Schmidt, R.A.M., 1963, Pleistocene marine microfauna in the Bootlegger Cove Clay, Anchorage Area, Alaska: Science, v. 141, p. 350-351.

Schmoll, H.R., and Dobrovlny, E., 1972, Generalized geologic map of Anchorage and vicinity, Alaska: U.S. Geological Survey Map I-787-A, scale 1:24,000, 1 sheet.

Schmoll, H.R., Szabo, B.J., Rubin, M., and Dobrovlny, E., 1972, Radiometric dating of marine shells from the Bootlegger Cove Clay, Anchorage area, Alaska: Geological Society of America Bulletin, v. 83, p. 1107-1114.

Seed, H.B., and Chan, C., 1964, Pulsating load tests on samples of clay and silt from Anchorage, Alaska, in Report on Anchorage area soil studies, to the U.S. Army Engineer District, Anchorage, Alaska: Seattle, Wash., 109 p.

Seed, H.B., and Idriss, I.M., 1970, Soil moduli and damping factors for dynamic response and analyses: University of California, Berkeley, Earthquake Engineering Research Institute Report No. 70-10, 34 p.

Seed, H.B., and Wilson, S.D., 1967, The Turnagain Heights landslide, Anchorage, Alaska: Journal of the Soil Mechanics and Foundation Division, American Society of Civil Engineers, v. 93, p. 325-353.

Shannon and Wilson, Inc., 1964, Report on Anchorage area soil studies, Alaska: Seattle, Wash., Shannon and Wilson, Inc., 109 p.

Updike, R.G., 1983, Seismic liquefaction potential in the Anchorage area, south-central Alaska: Geological Society of America Abstracts with Programs, v. 15, no. 5, p. 374.

\_\_\_\_\_, 1984, The Turnagain Heights landslide—an assessment using the electric cone penetration test: Alaska Division of Geological and Geophysical Surveys Report of Investigations 84-13, 48 p.

\_\_\_\_\_, 1986, Engineering geologic maps, Government Hill area, Anchorage, Alaska: U.S. Geological Survey Map I-1610, scale 1:4800, 1 sheet.

Updike, R.G., and Carpenter, B.A., 1986, Engineering geology of the Government Hill area, Anchorage, Alaska: U.S. Geological Survey Bulletin 1588, 32 p.

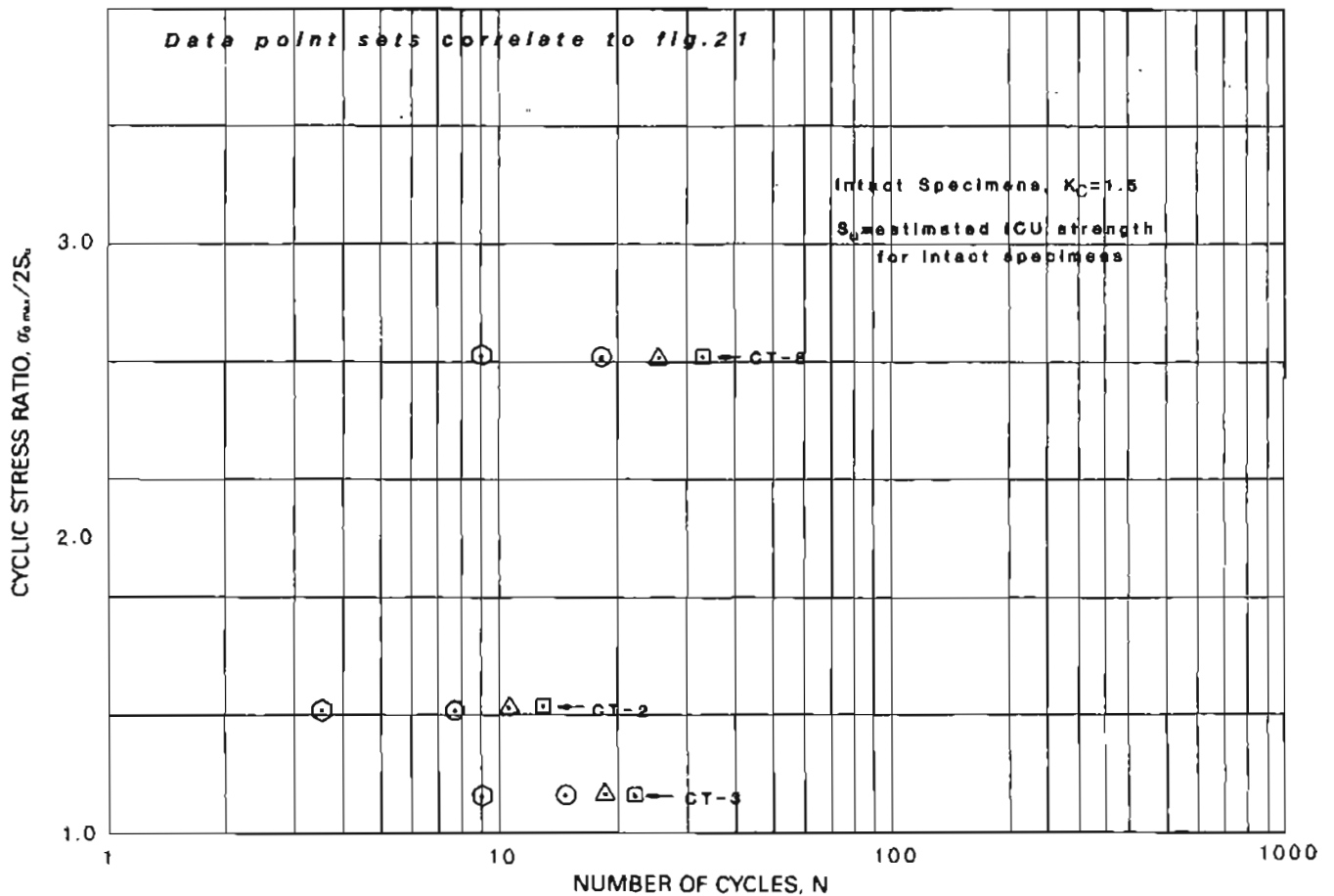


**Figure 22.** Cyclic stress ratio (estimated from isotropically consolidated-undrained tests) versus number of cycles, for three intact specimens under initial consolidation ratio of 1.5.

Updike, R.G., Cole, D.A., and Ulery, C.A., 1982, Shear moduli and damping ratios for the Bootlegger Cove Formation as determined by resonant-column testing: Alaska Division of Geological and Geophysical Surveys Geologic Report 73, p. 7-12.

Updike, R.G., and Ulery, C.A., 1983, Preliminary geologic map of Anchorage B-6 NW (Eklutna Lake) Quadrangle: Alaska Division of Geological and Geophysical Surveys Geologic Report of Investigations 83-8, scale 1:10,000, 2 sheets.

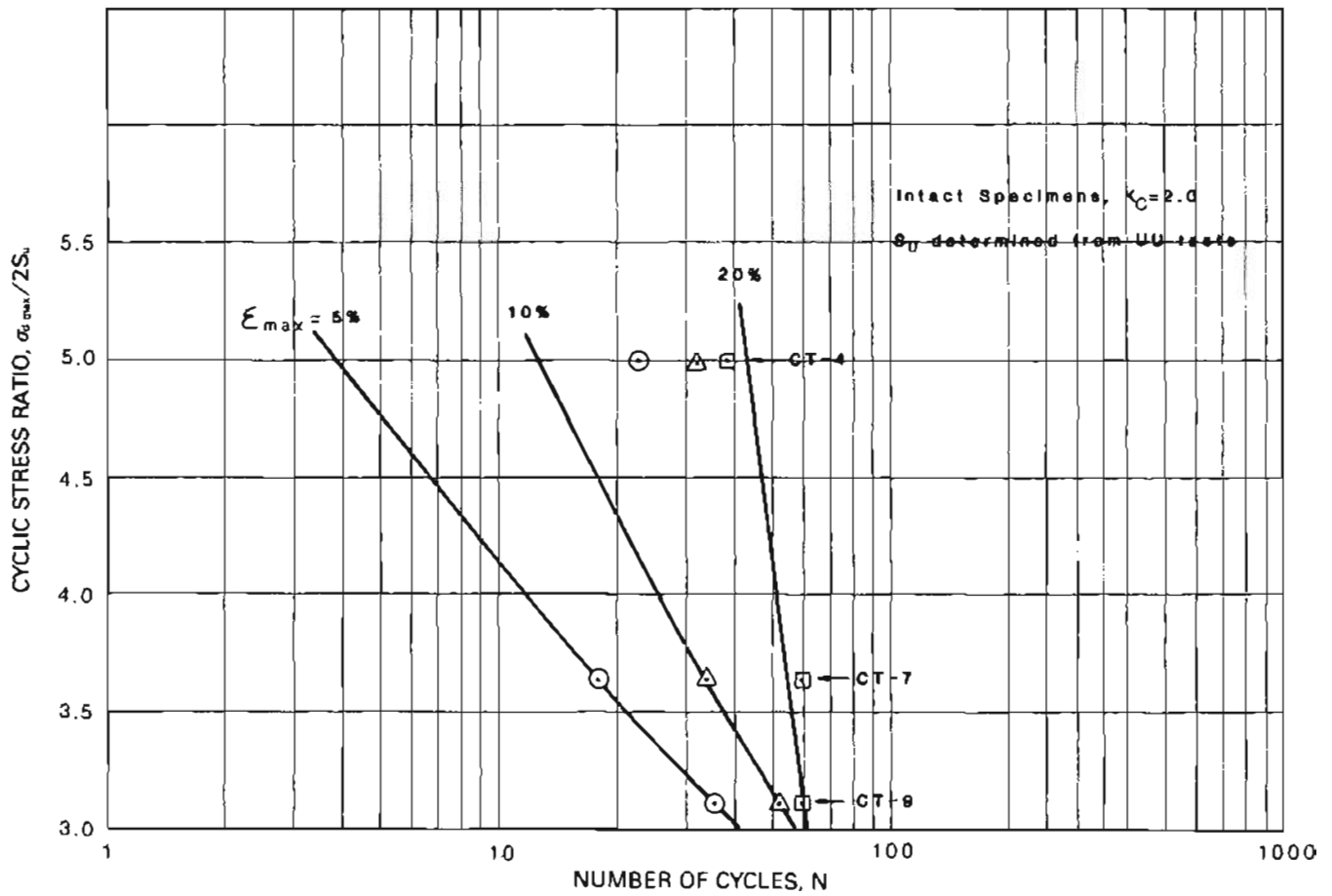


Figure 23. Cyclic stress ratio (determined from unconsolidated-undrained tests) versus number of cycles, for three intact specimens under initial consolidation ratio of 2.0.

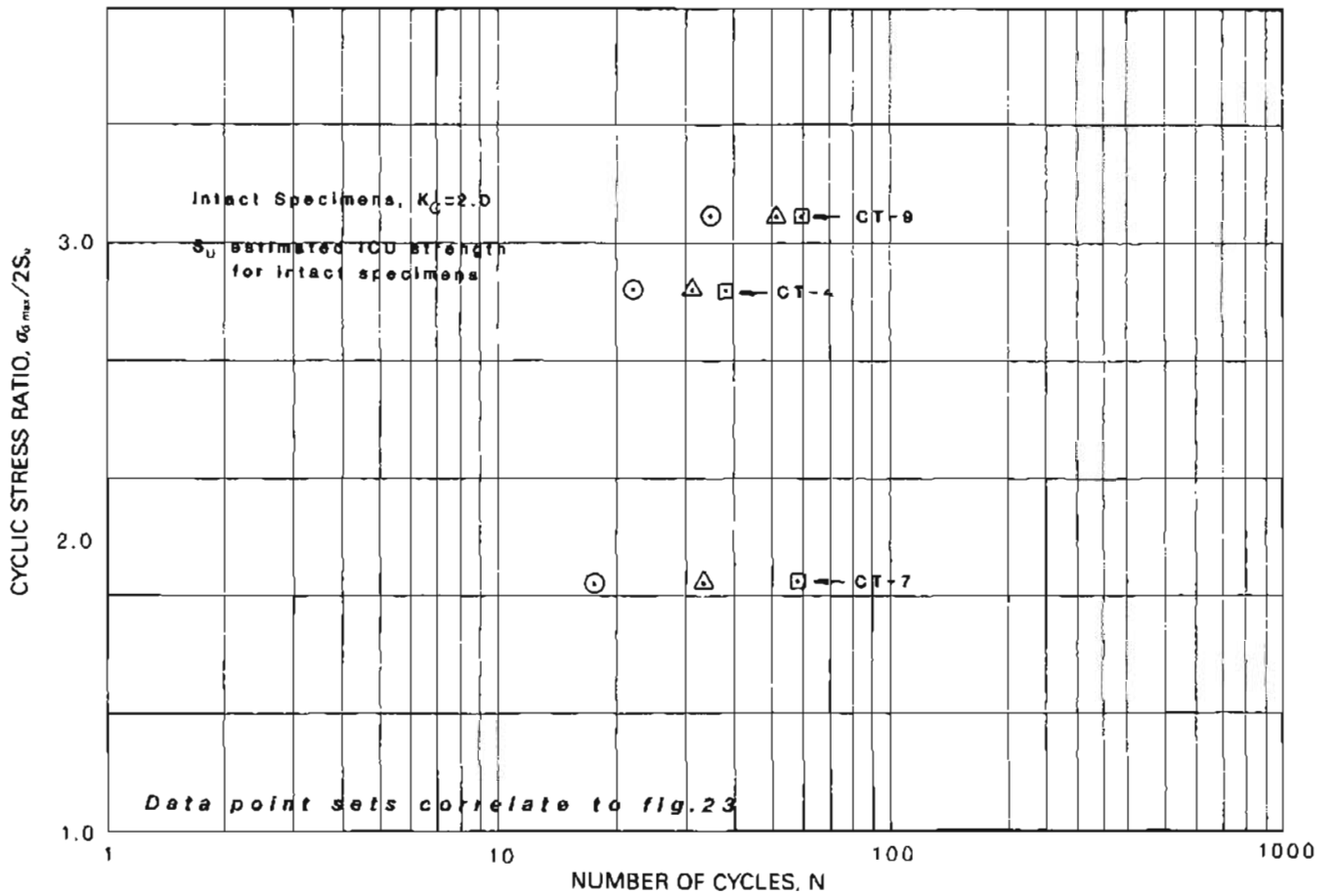
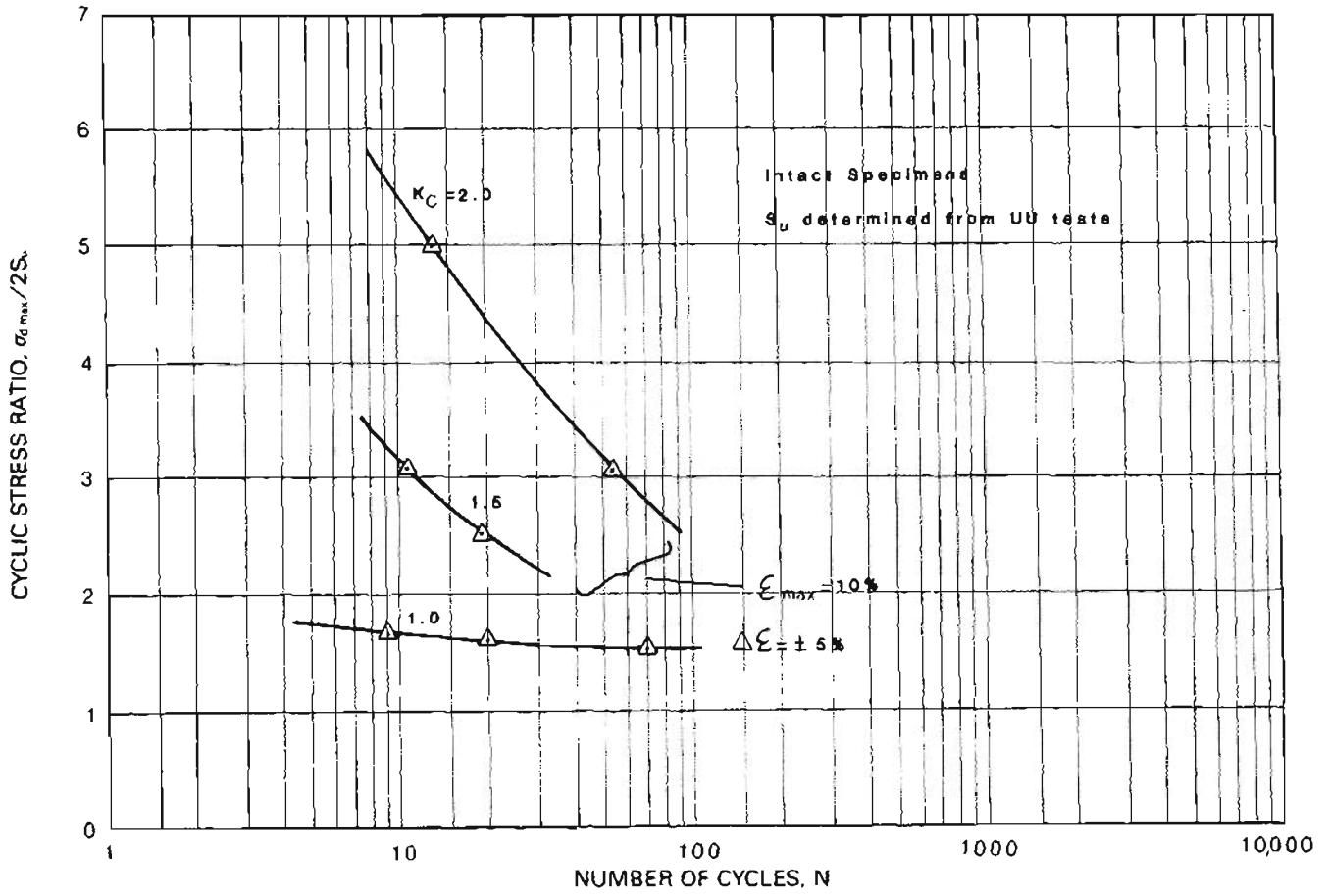


Figure 24. Cyclic stress ratio (estimated from isotropically consolidated-undrained tests) versus number of cycles, for three intact specimens, all at initial consolidation ratios of 2.0.



**Figure 25.** Cyclic stress ratio versus number of cycles for seven intact specimens at consolidation ratios of 1.0, 1.5, and 2.0. Maximum strains of 5 percent (for  $K_c = 1.0$ ) and 10 percent (for  $K_c = 1.5$  and 2.0) were taken from figures 17, 21, and 23, which were based on unconsolidated-undrained tests.

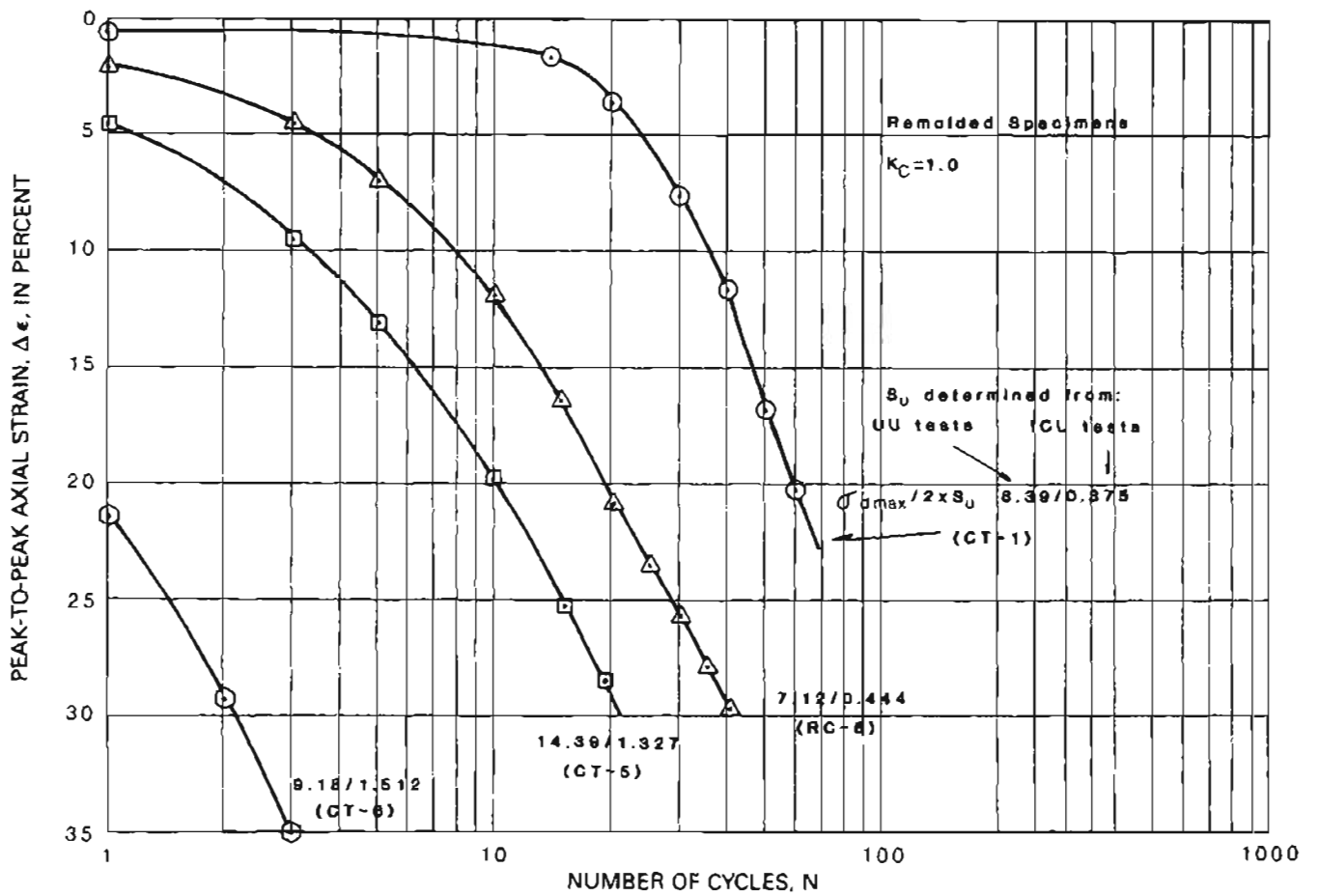


Figure 26. Peak-to-peak axial strain versus number of cycles for four remolded specimens, all at initial consolidation ratios of 1.0.

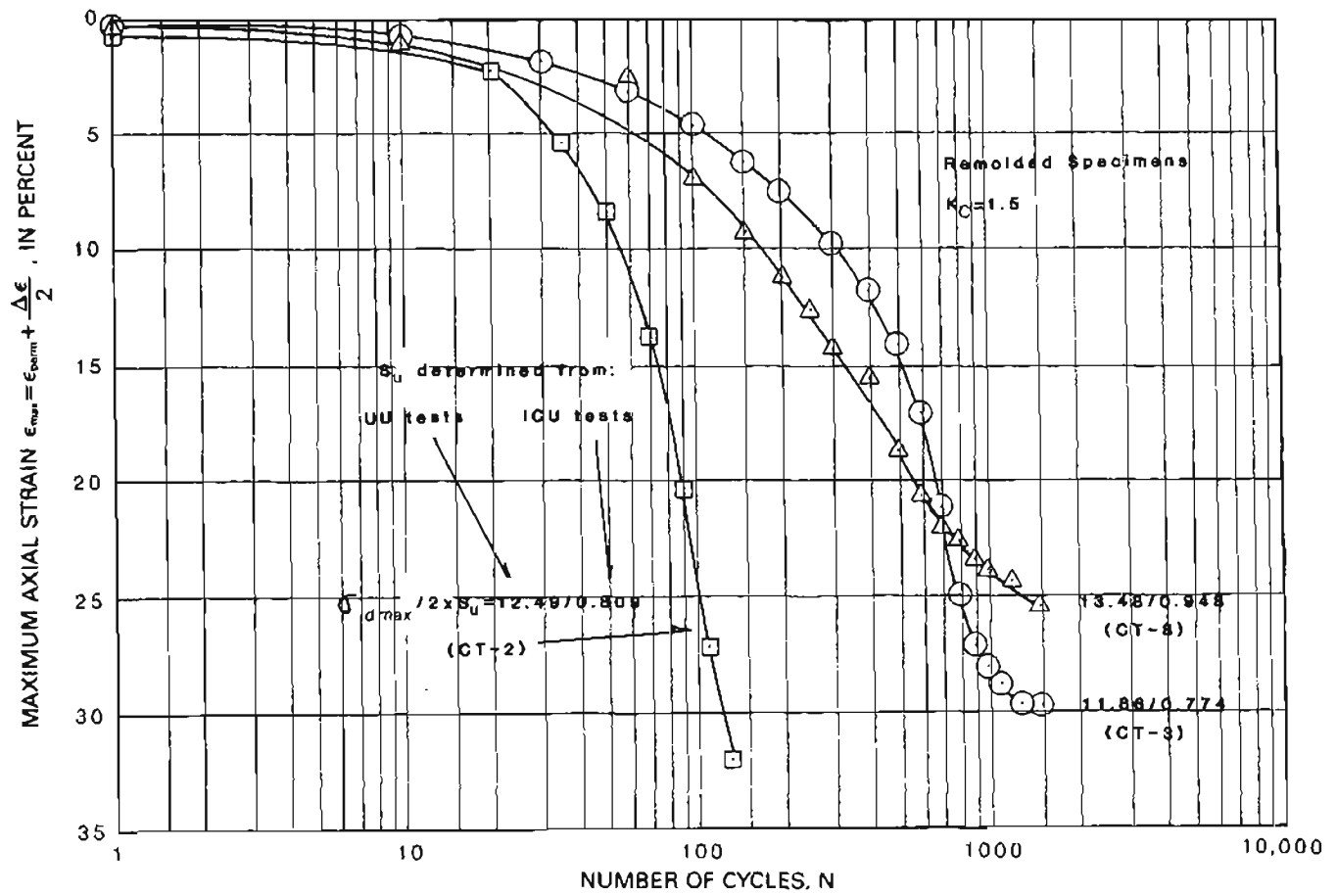


Figure 27. Maximum axial strain versus number of cycles for three remolded specimens, all at initial consolidation ratios of 1.5.

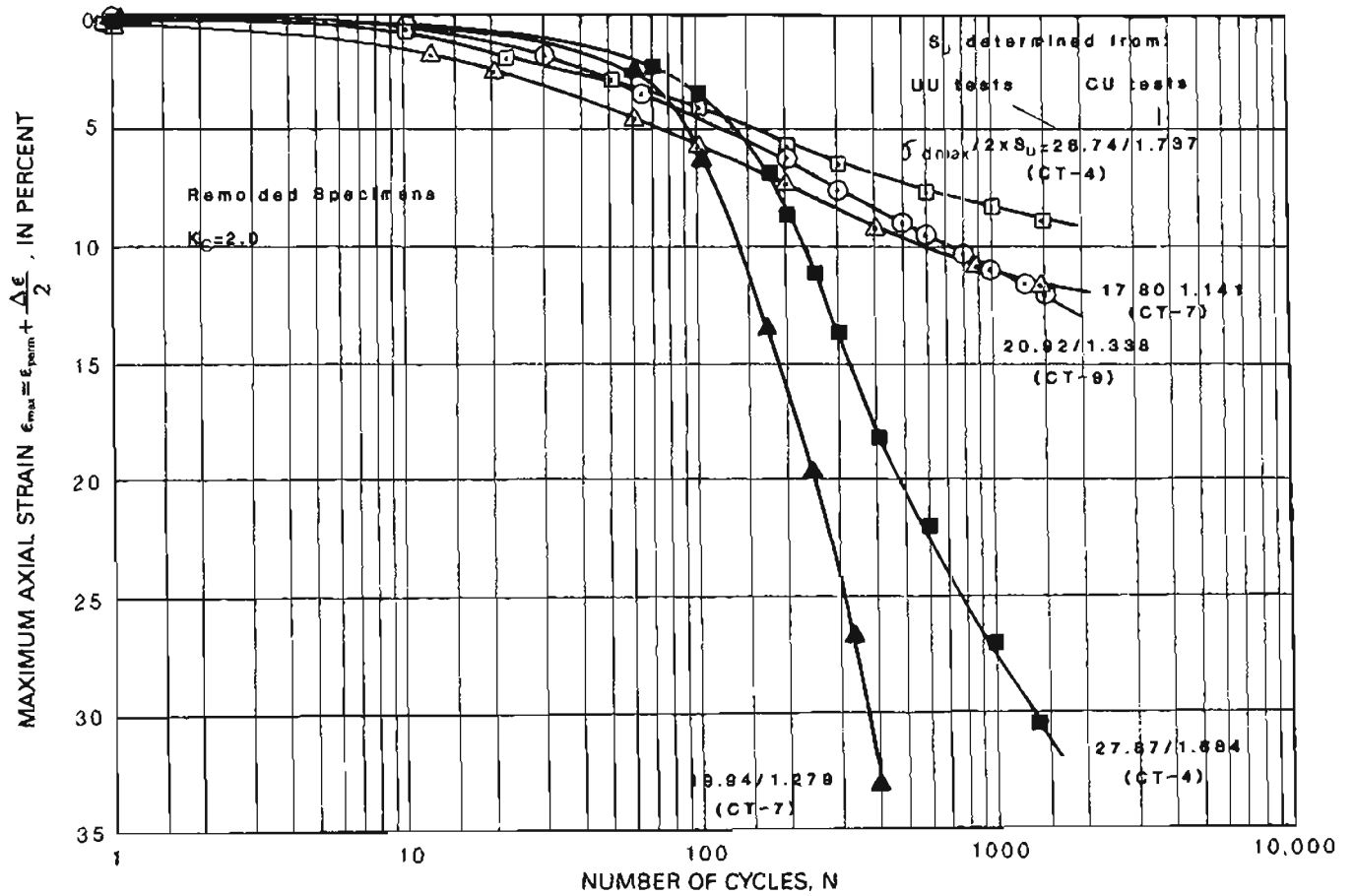


Figure 28. Maximum axial strain versus number of cycles for five remolded specimens, all at initial consolidation ratios of 2.0.

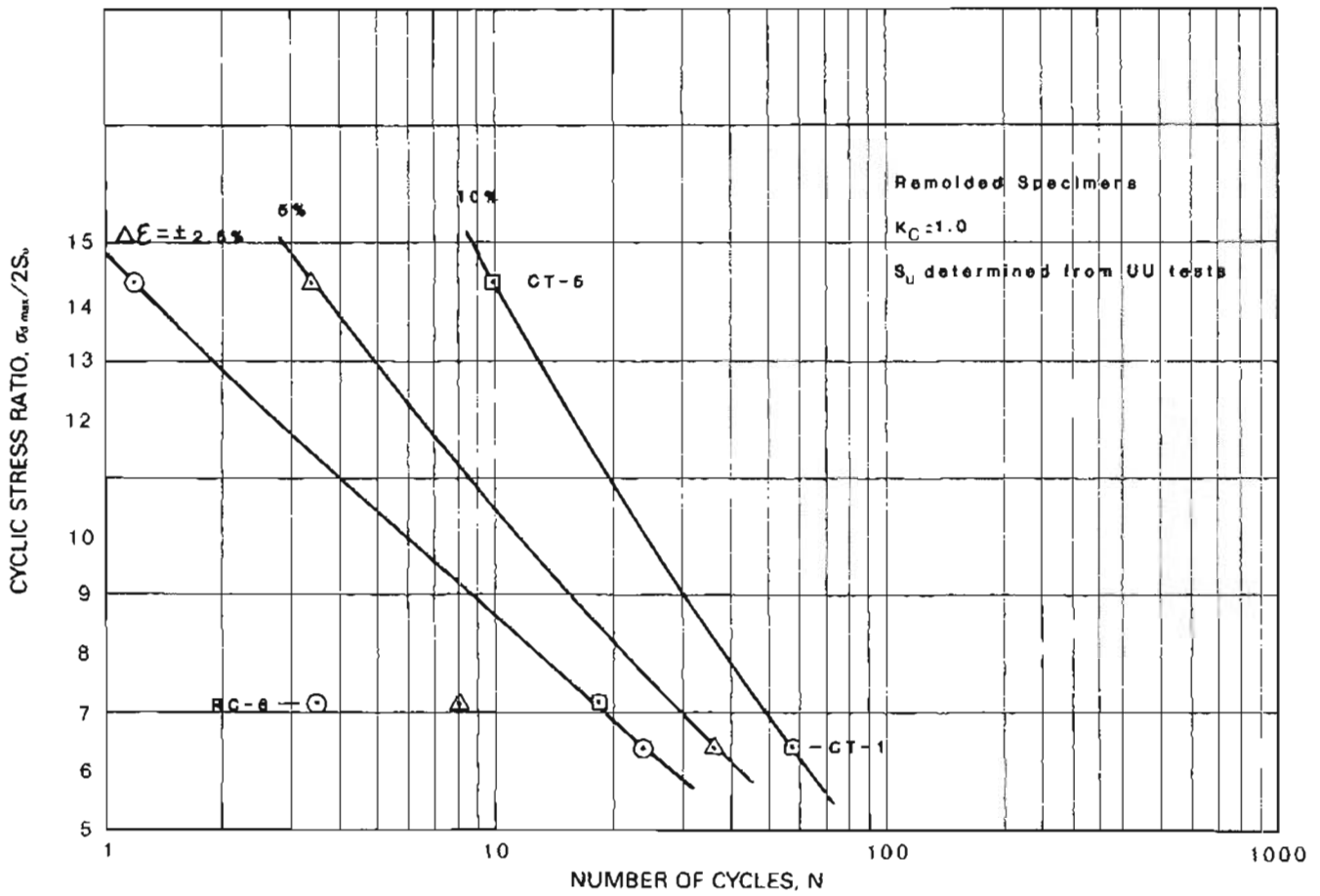


Figure 29. Cyclic stress ratio (determined using unconsolidated-undrained tests) versus number of cycles, for three remolded specimens, under initial consolidation ratios of 1.0.

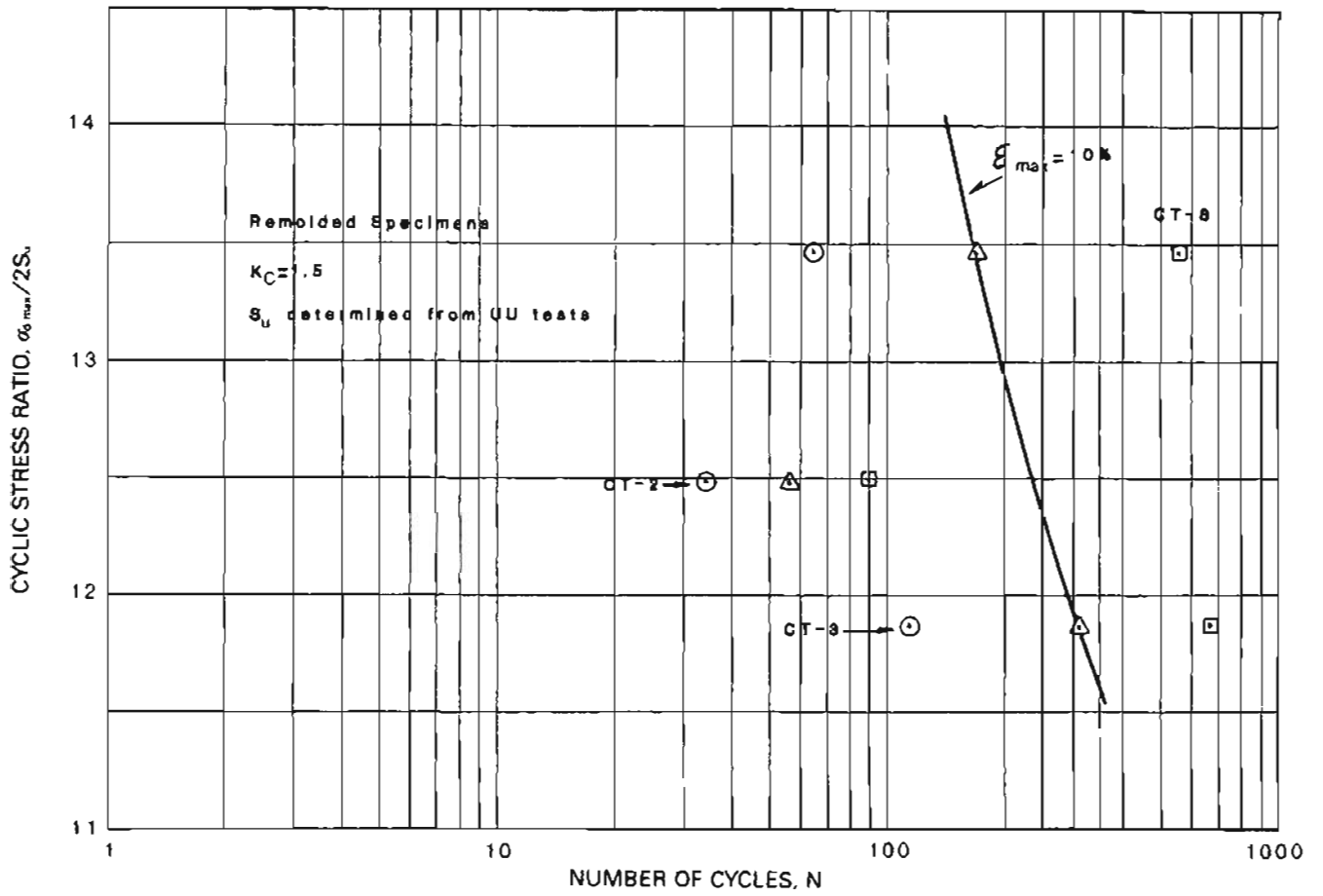


Figure 30. Cyclic stress ratio (determined using unconsolidated-undrained tests) versus number of cycles, for three remolded specimens, under initial consolidation ratios of 1.5.

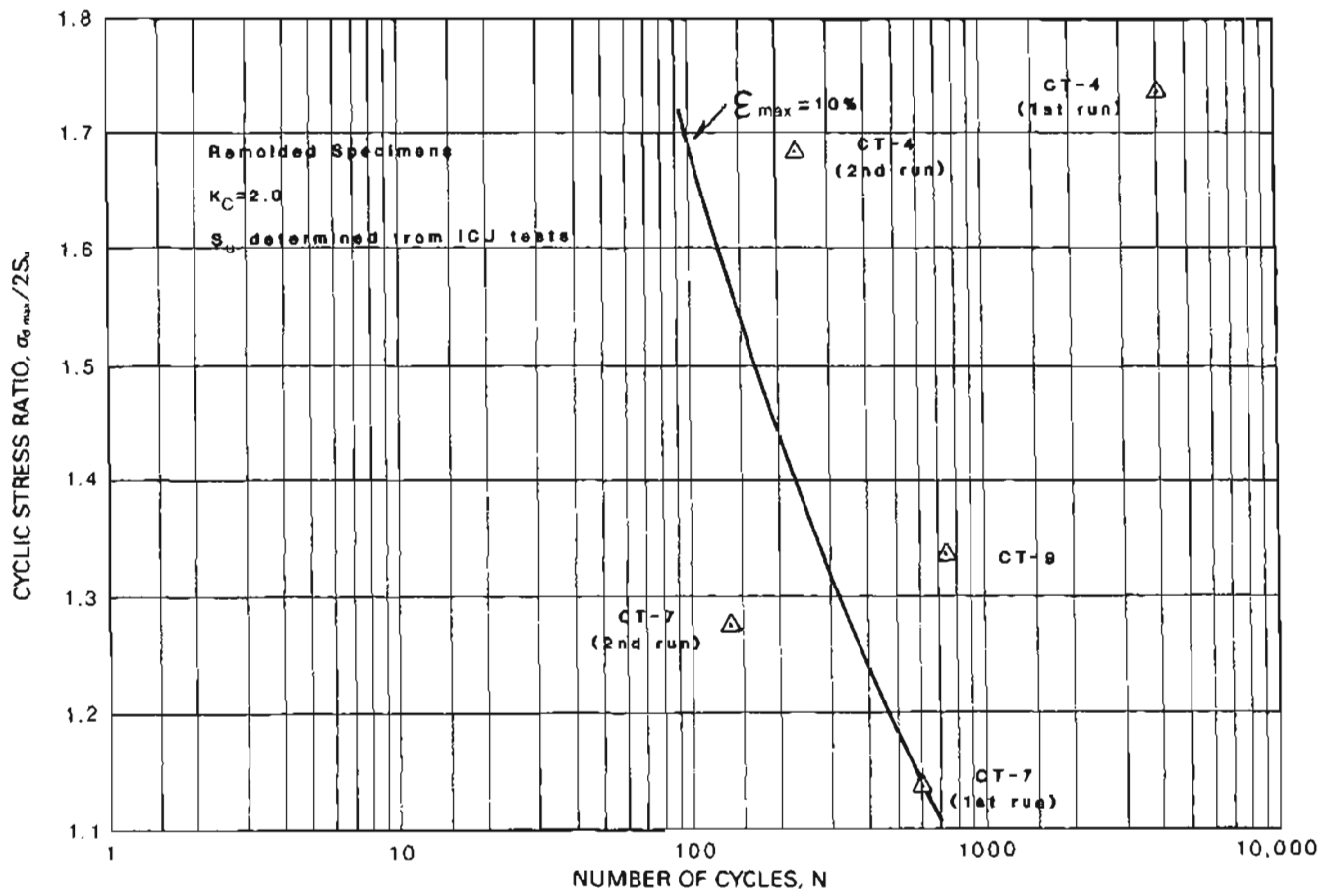


Figure 31. Cyclic stress ratio (determined using unconsolidated-undrained tests) versus number of cycles, for four remolded specimens, under initial consolidation ratios of 2.0.

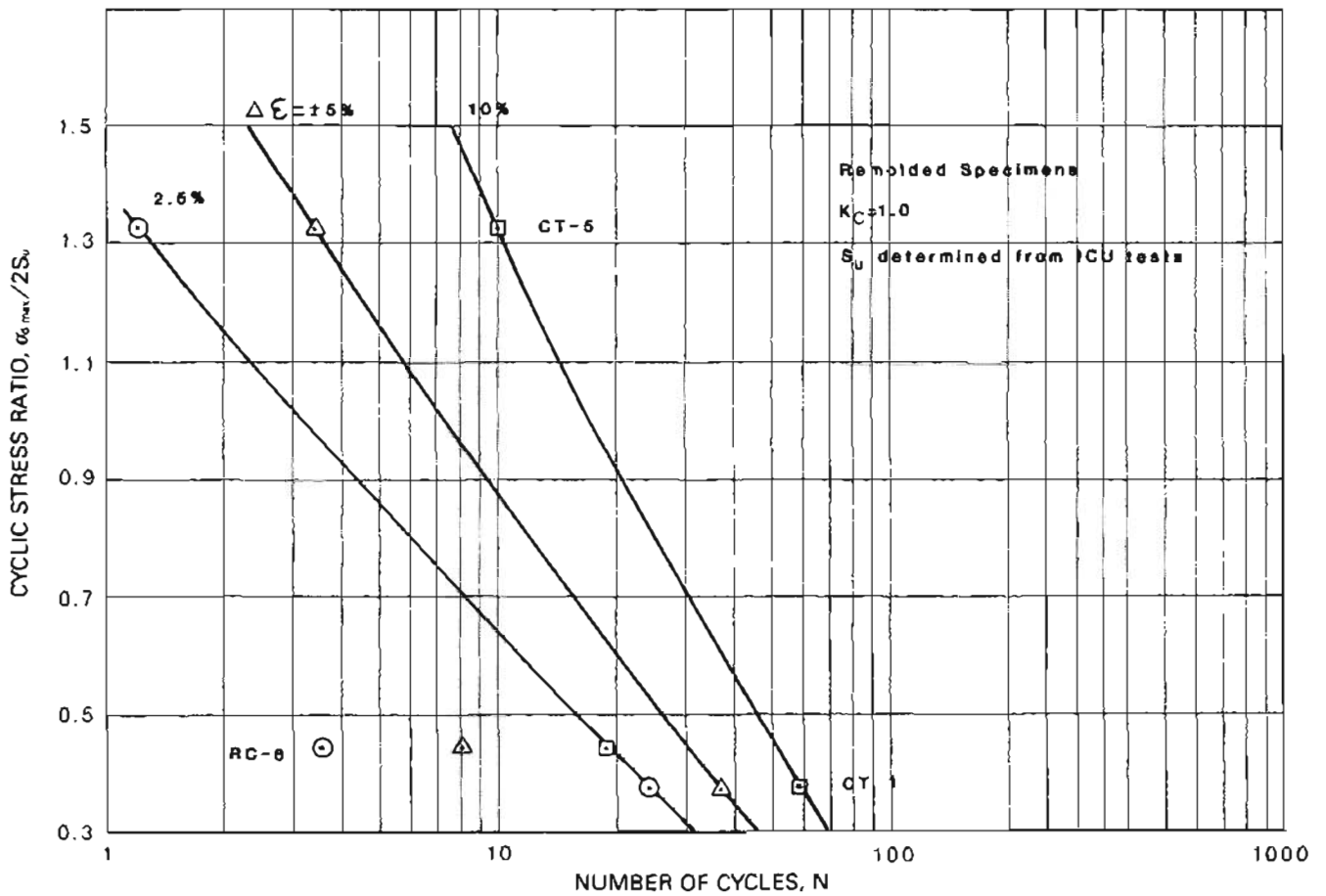


Figure 32. Cyclic stress ratio (determined using isotropically consolidated-undrained tests) versus number of cycles, for three remolded specimens, under initial consolidation ratios of 1.0.

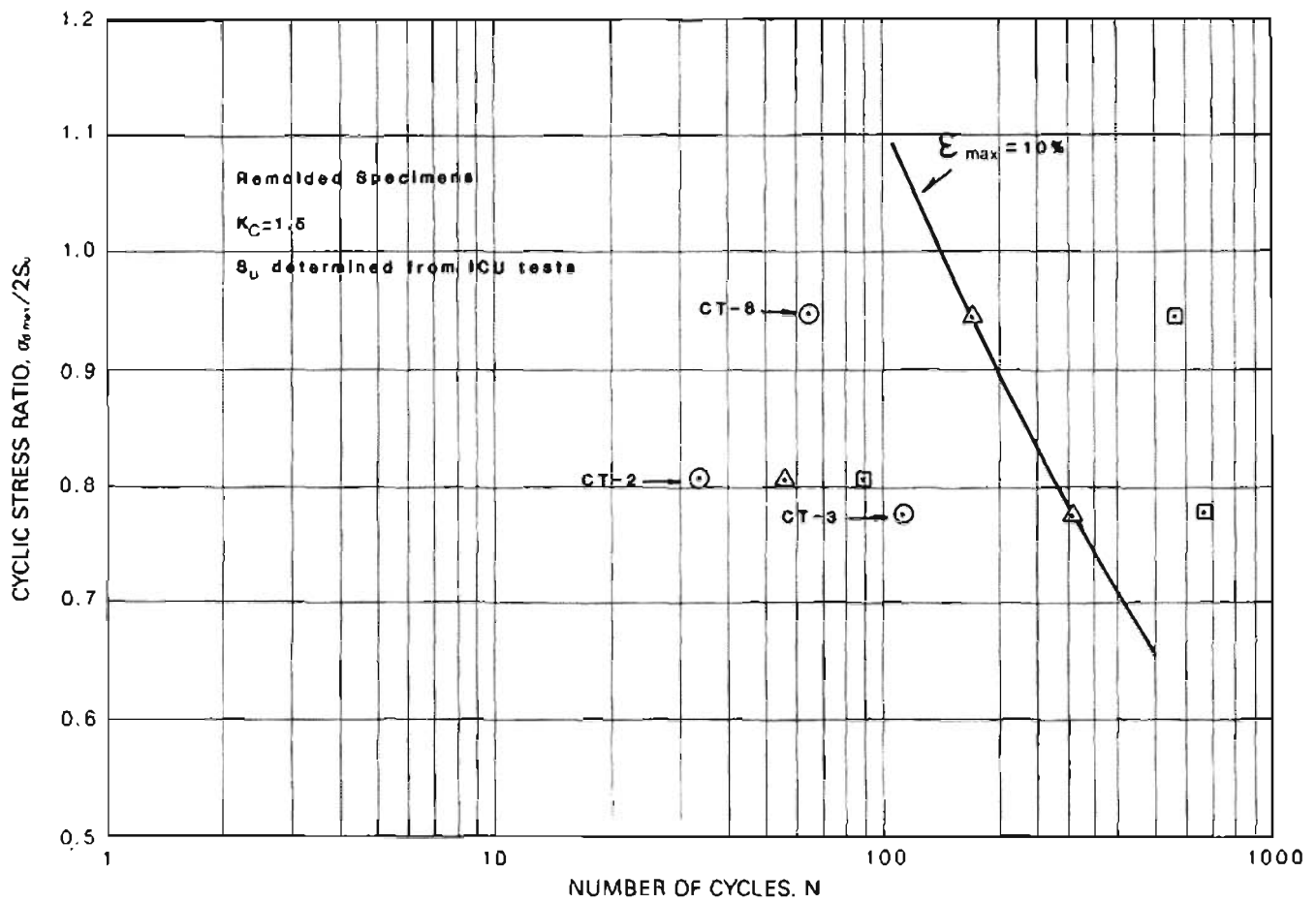


Figure 33. Cyclic stress ratio (determined using isotropically consolidated-undrained tests) versus number of cycles for three remolded specimens, under initial consolidation ratios of 1.5.

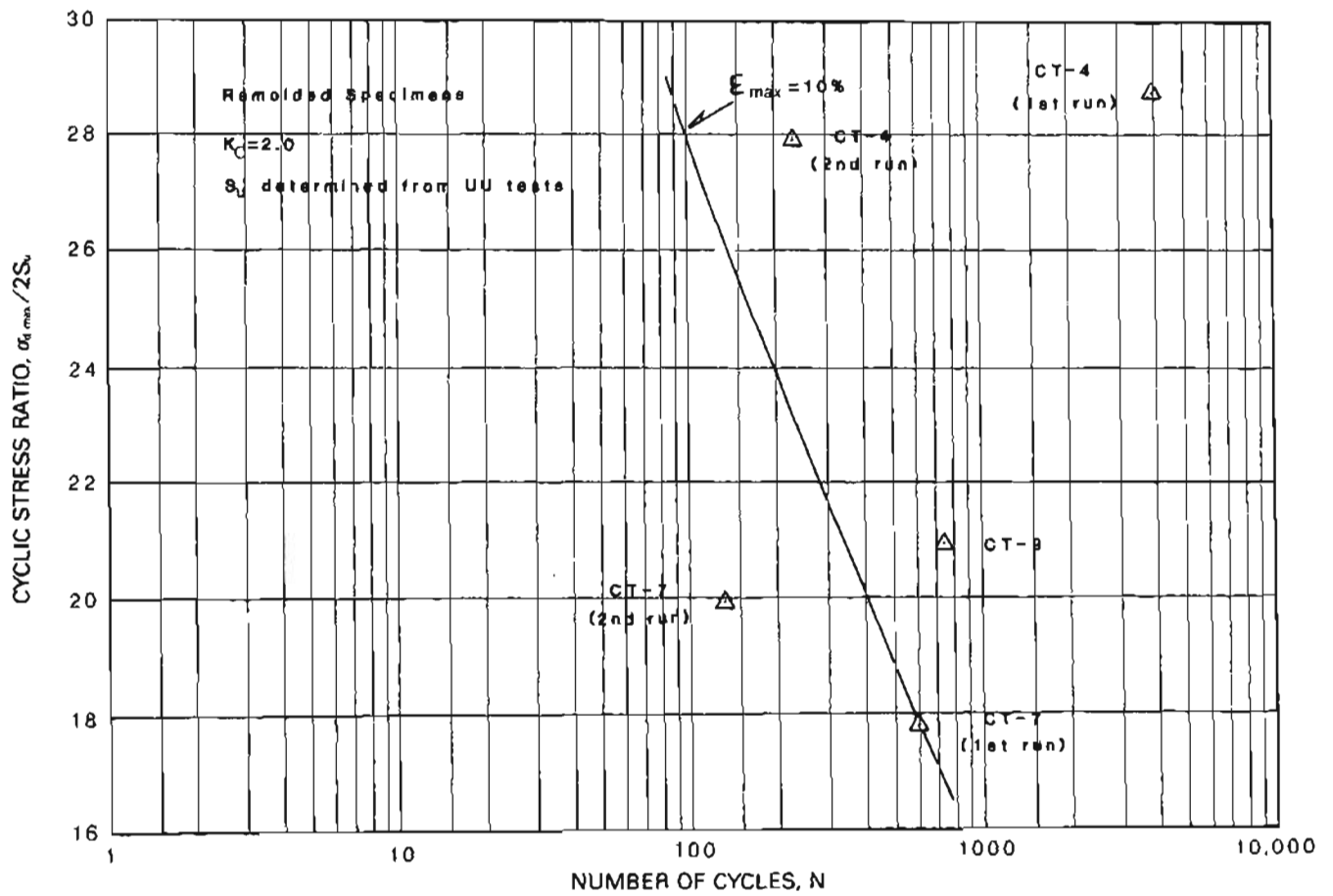
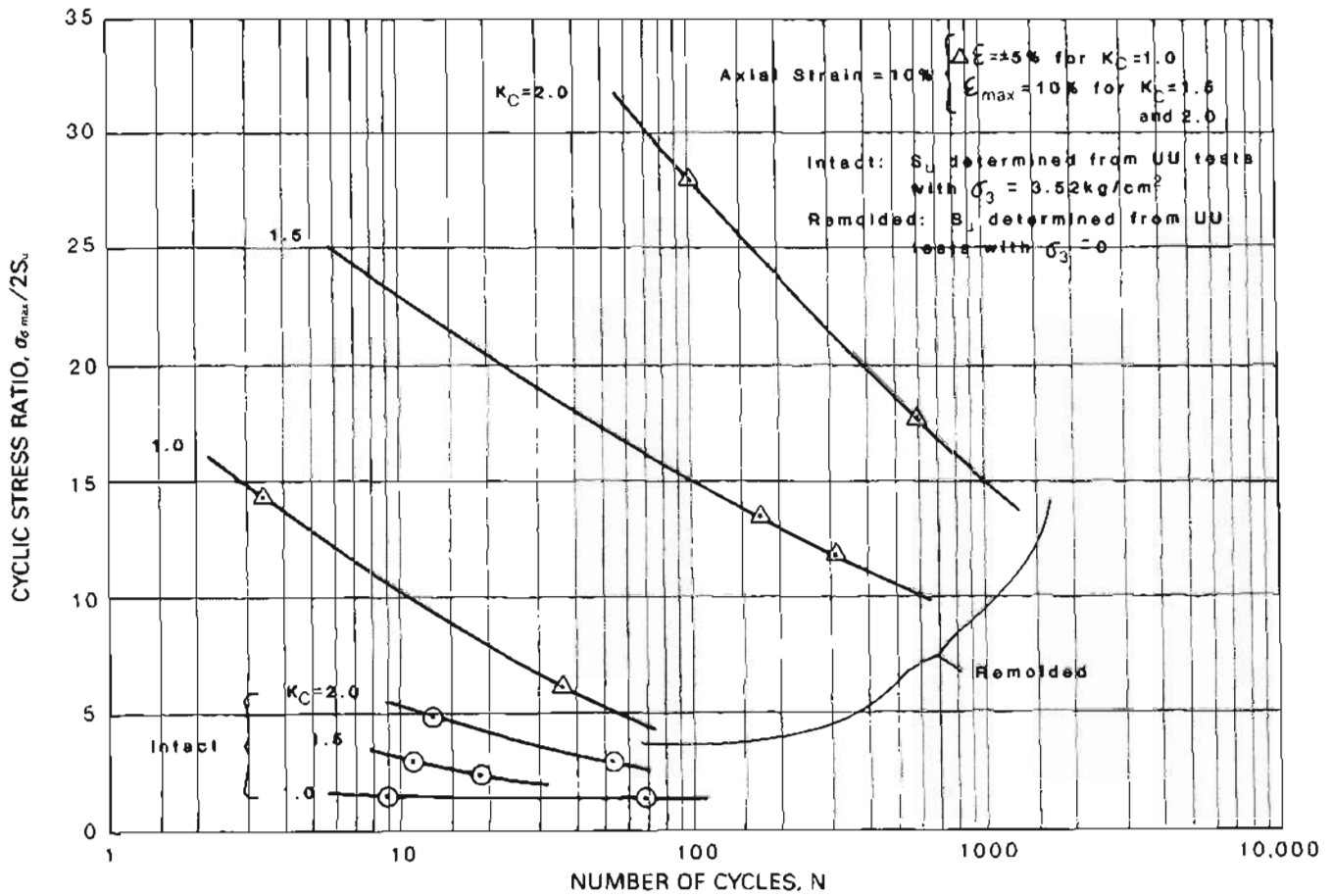


Figure 34. Cyclic stress ratio (determined using isotropically consolidated-undrained tests) versus number of cycles for four remolded specimens, under initial consolidation ratios of 2.0.



**Figure 35.** Cyclic stress ratio versus number of cycles for six remolded specimens at consolidation ratios of 1.0, 1.5, and 2.0. Axial strains of 5 percent (for  $K_c = 1.0$ ) and 10 percent (for  $K_c = 1.5$  and 2.0) were taken from figures 29, 30, and 31 (UU tests). Curves for intact specimens, as shown in figure 25, are given for comparison.

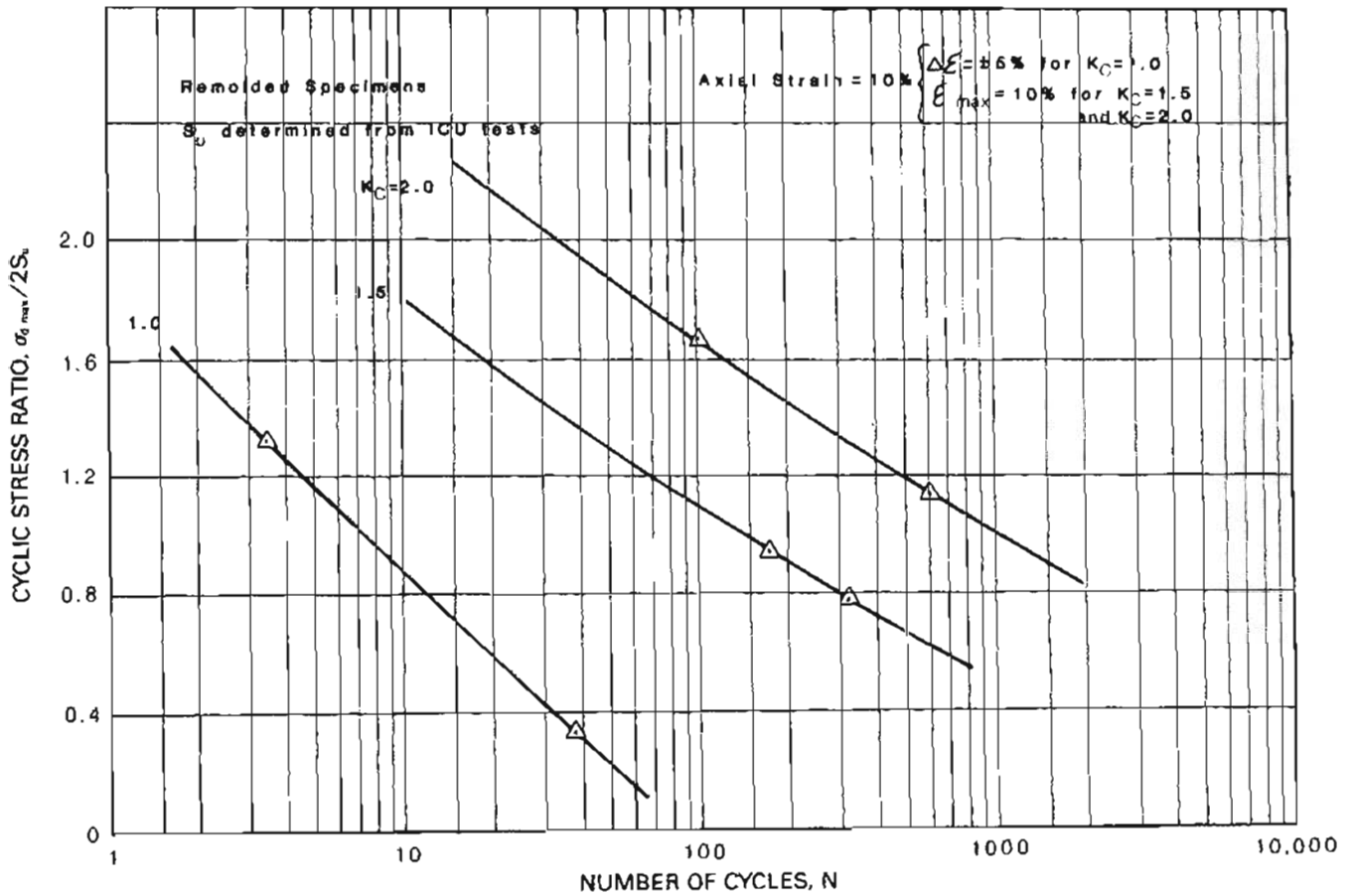


Figure 36. Cyclic stress ratio versus number of cycles for remolded specimens at  $K_c = 1.0, 1.5,$  and  $2.0,$  based upon shear strengths determined by isotropically consolidated-undrained conditions.

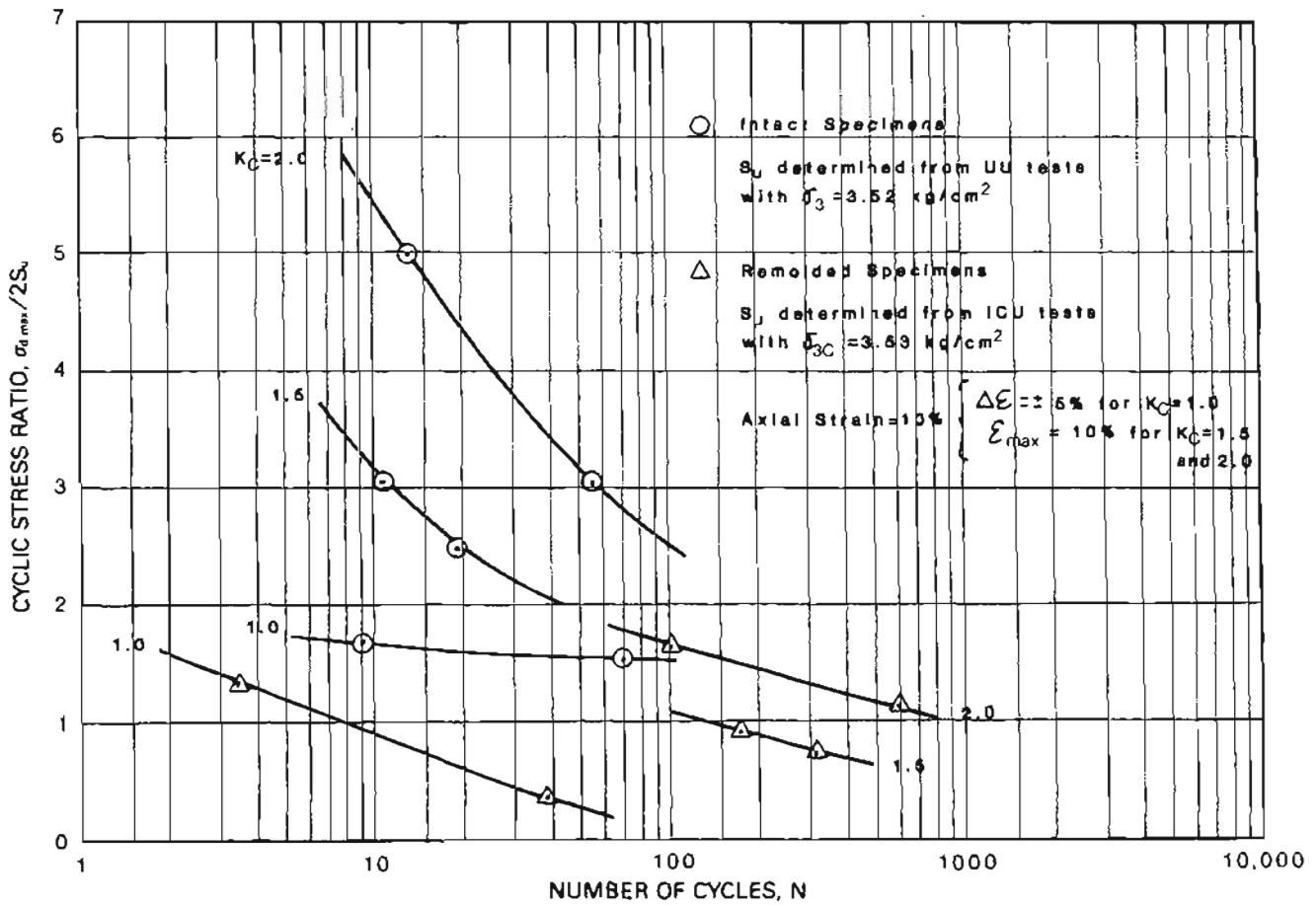
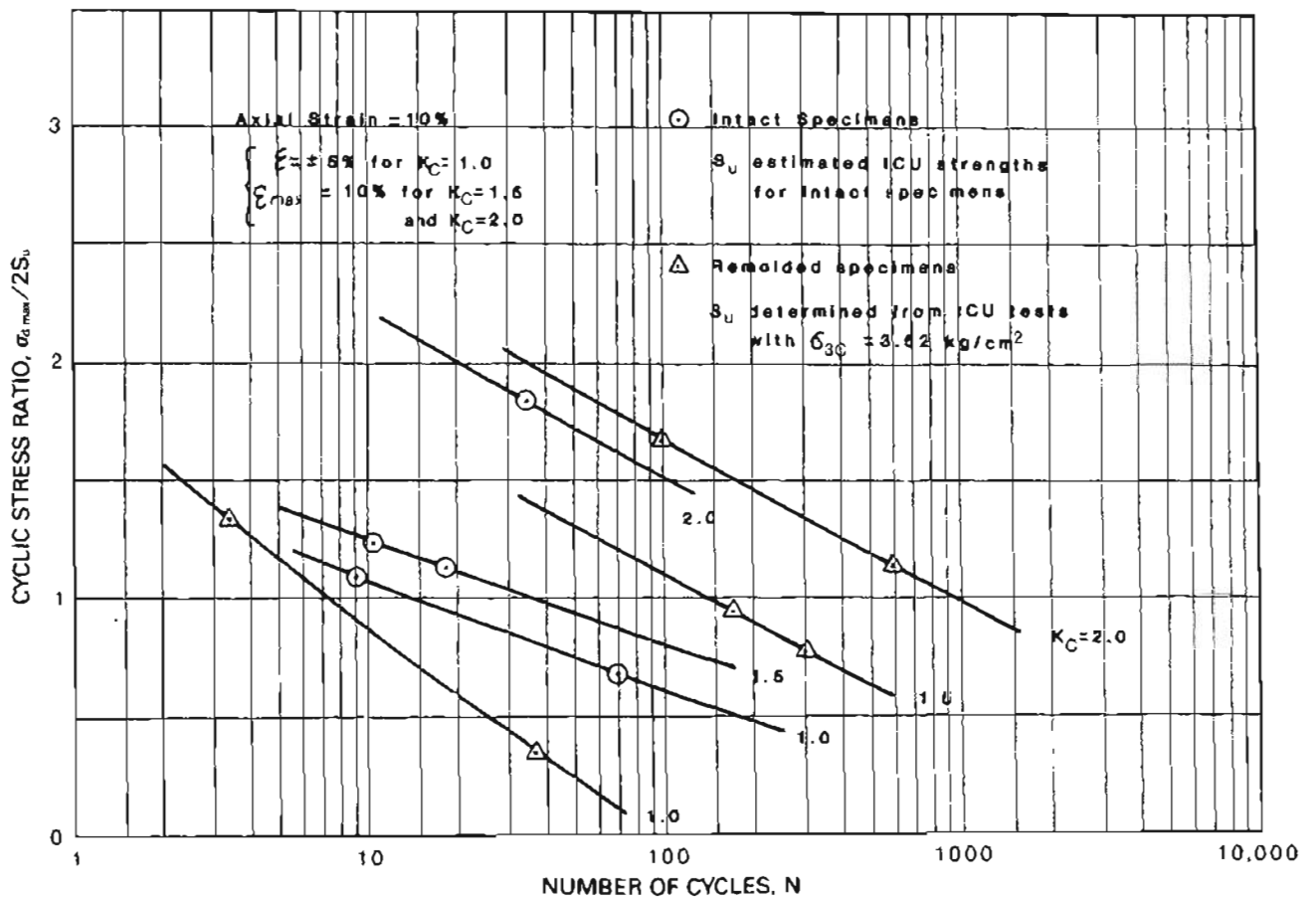


Figure 37. A comparison of cyclic stress ratios for intact specimens (determined from unconsolidated-undrained tests) with ratios of remolded specimens (determined from isotropically consolidated-undrained tests). Note apparent lower strength of remolded specimens at all consolidation ratios.



**Figure 38.** A comparison of cyclic stress ratios for intact specimens (estimated from isotropically consolidated-undrained (ICU) tests) with ratios for remolded specimens (measured from ICU tests). In contrast to figure 37, a much closer agreement in strength between intact and remolded specimens is shown in this graph.

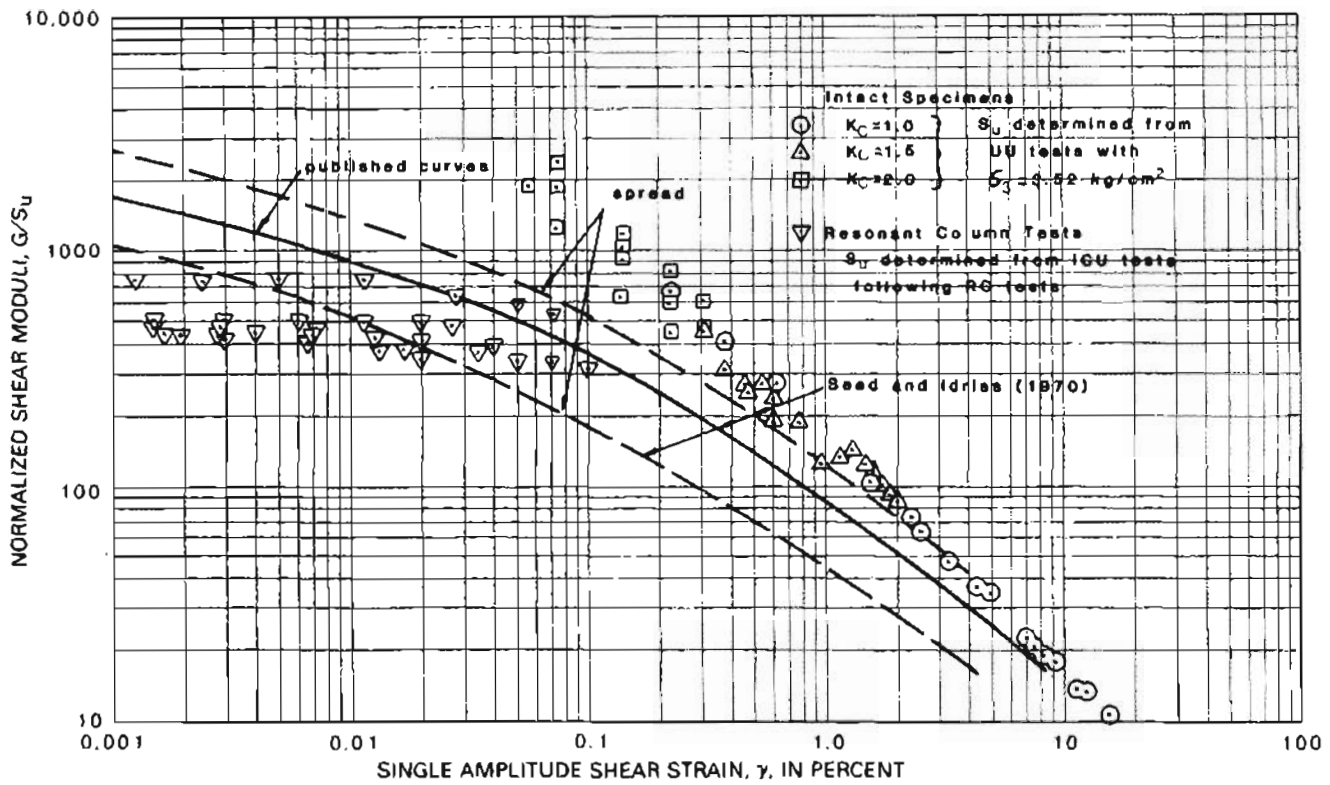


Figure 39. Normalized shear moduli for intact specimens using shear strengths determined by unconsolidated-undrained tests. Also shown are moduli results from resonant column tests (see Updike and others, 1982) and normalized curves from Seed and Idriss (1970).

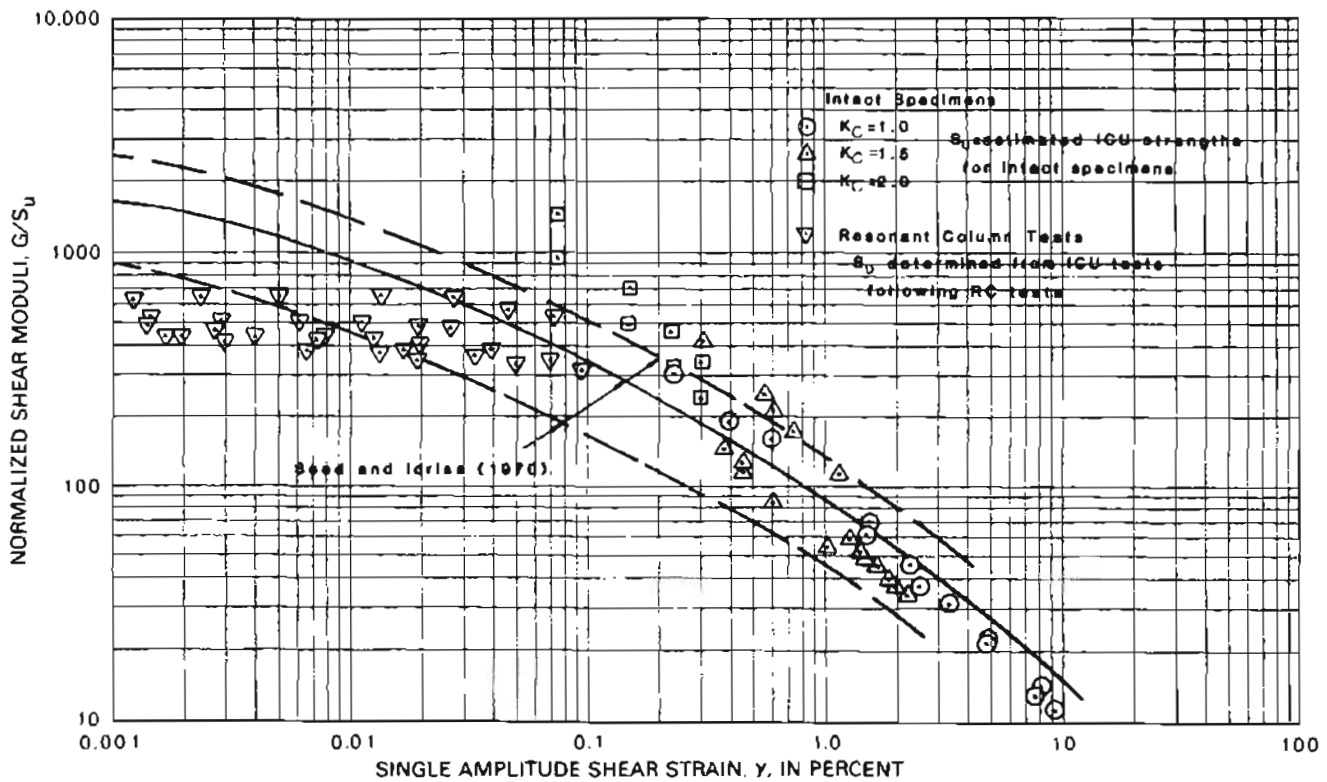


Figure 40. Normalized shear moduli for intact specimens using shear strengths determined by estimates of isotropically consolidated-undrained shear tests. Also shown are moduli results from resonant column tests (see Updike and others, 1982) and normalized curves from Seed and Idriss (1970).

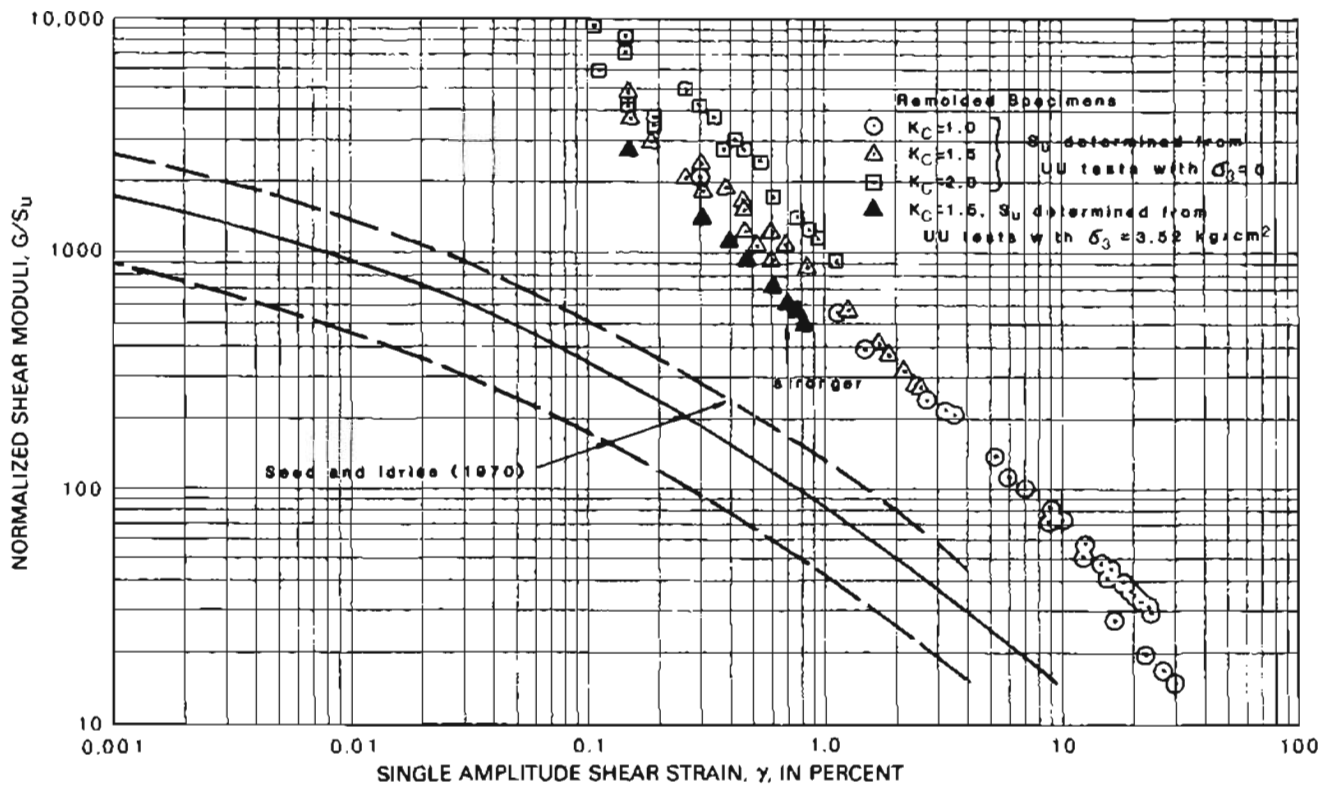


Figure 41. Normalized shear moduli for remolded specimens using shear strengths determined from unconsolidated-undrained tests. Note the two different confining pressures,  $\sigma_3$ , for a consolidation ratio of 1.5. Data points suggest higher strength than the Seed and Idriss (1970) normalized moduli curves would suggest.

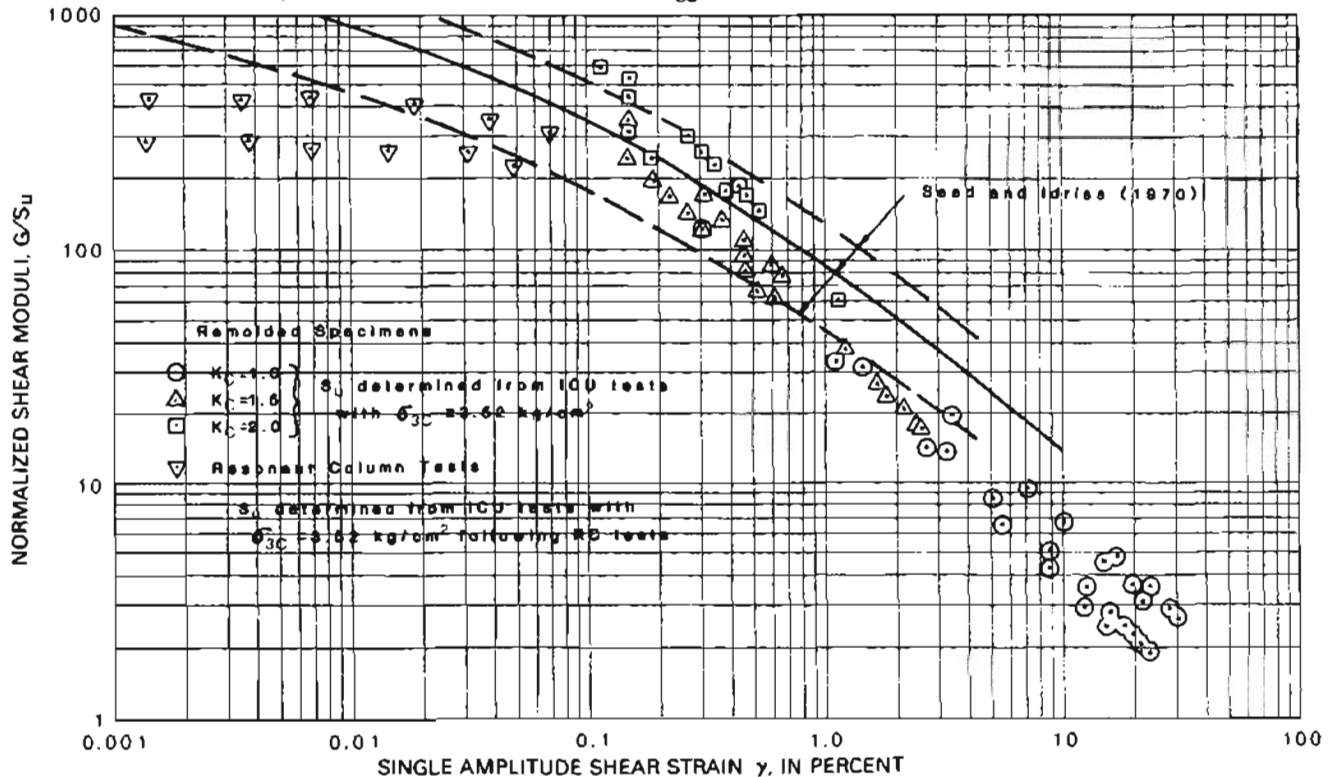


Figure 42. Normalized shear moduli for remolded specimens using shear strengths determined from isotropically consolidated-undrained (ICU) tests. The Seed and Idriss (1970) moduli curves from figure 41 are in much closer agreement with data points based upon ICU tests. The low-strain resonant column data points (from Updike and others, 1982) show reasonable continuity with the cyclic triaxial test data.

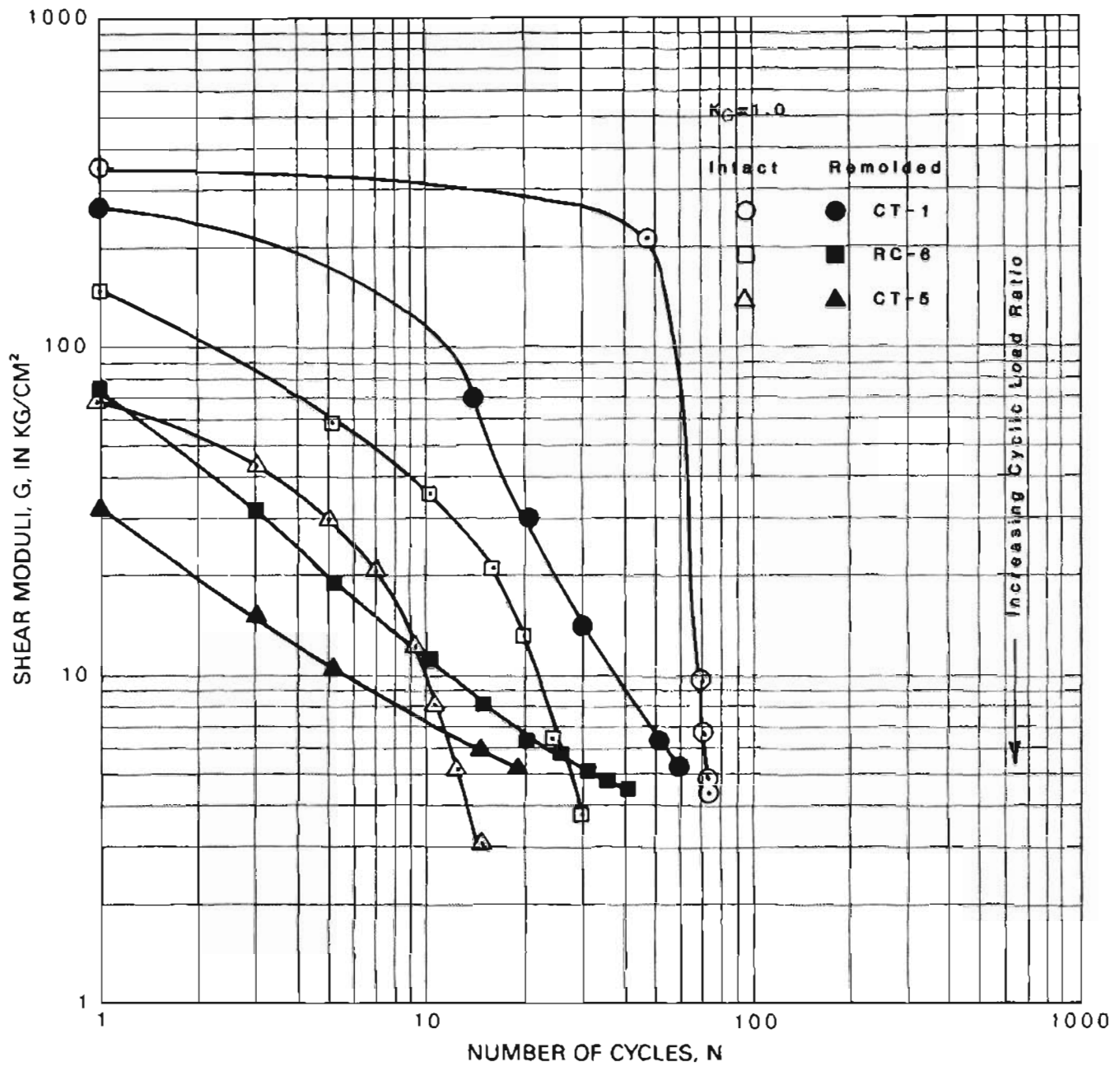


Figure 43. A comparison of shear moduli with respect to number of cycles for the intact and remolded states of three specimens, all at a consolidation ratio of 1.0. Specimens CT-1 and CT-5 represent facies F.IV of the Bootlegger Cove Formation; specimen RC-6 is from facies F.II of the Bootlegger Cove Formation.

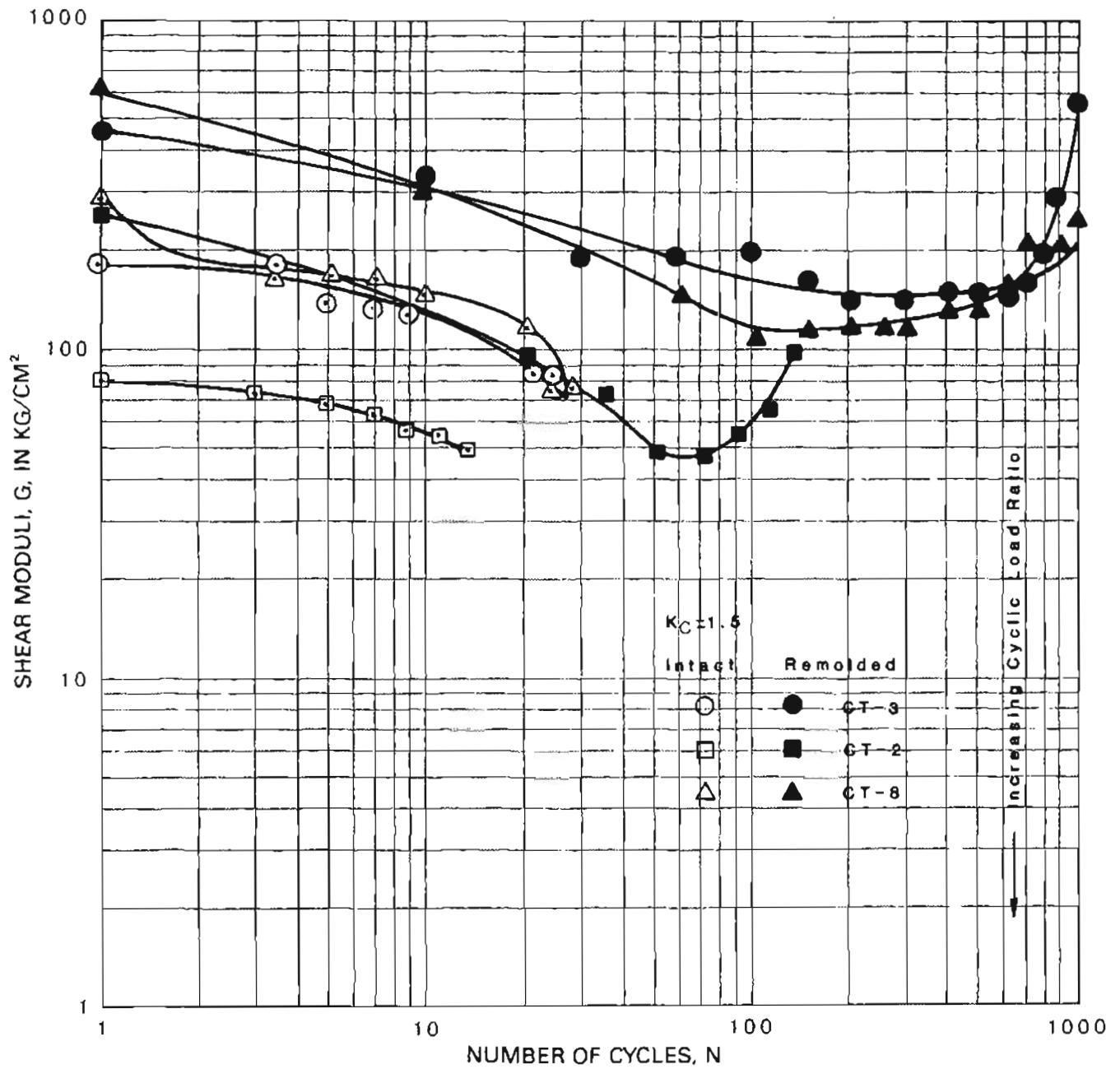
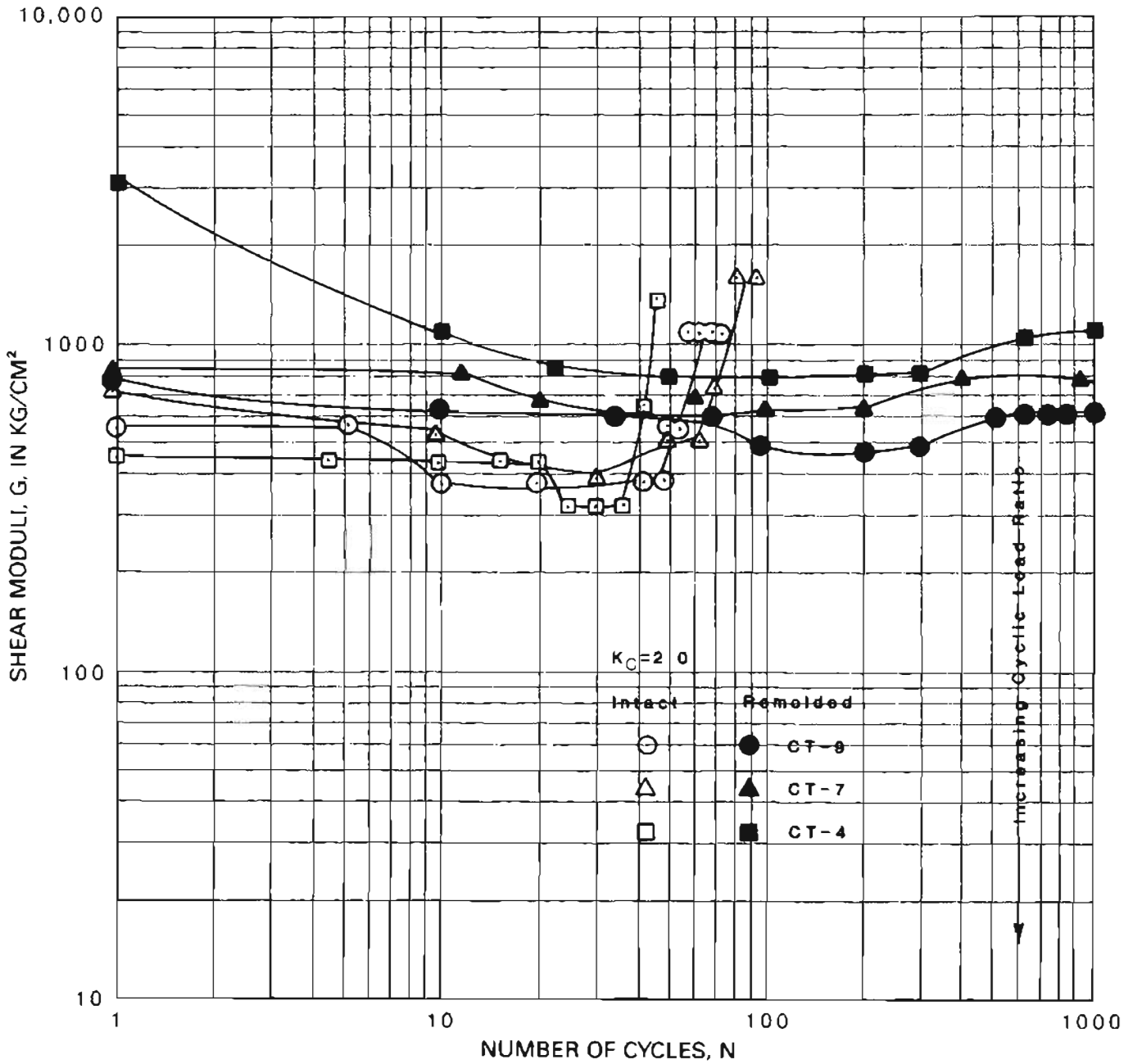


Figure 44. A comparison of shear moduli with respect to number of cycles for the intact and remolded states of three specimens, all at a consolidation ratio of 1.5. Specimens CT-2 and CT-8 represent facies F.II of the Bootlegger Cove Formation; specimen CT-3 is from facies F.III of the Bootlegger Cove Formation.



**Figure 45.** A comparison of shear moduli with respect to number of cycles for the intact and remolded states of three specimens, all at a consolidation ratio of 2.0. Specimens CT-4 and CT-7 represent facies F.IV of the Bootlegger Cove Formation; specimen CT-9 is from facies F.II of the Bootlegger Cove Formation.

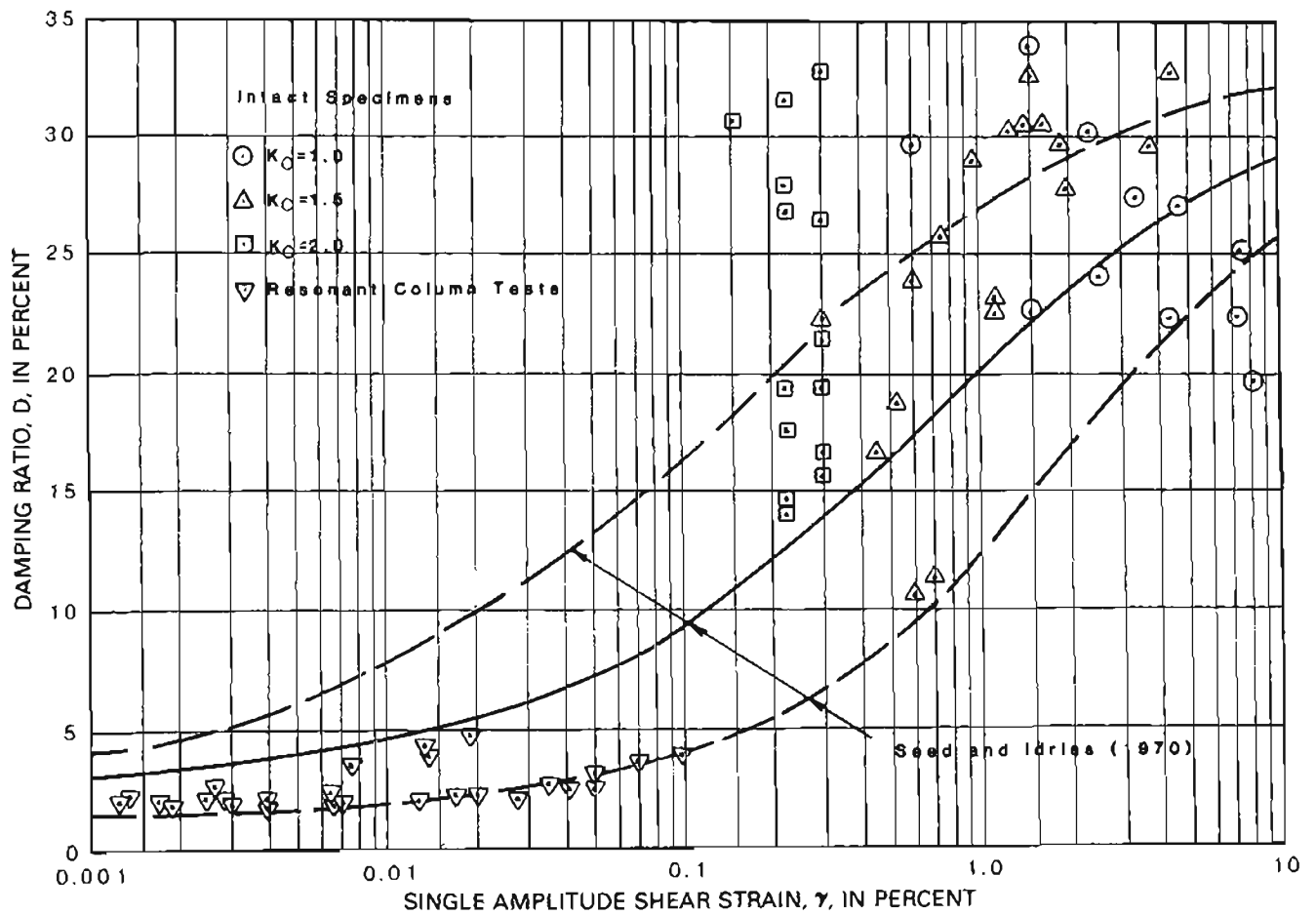


Figure 46. Damping ratios versus percent strain for intact specimens tested at various consolidation ratios. Damping ratio curves from Seed and Idriss (1970) and data points from resonant column tests (Updike and others, 1982) are also shown.

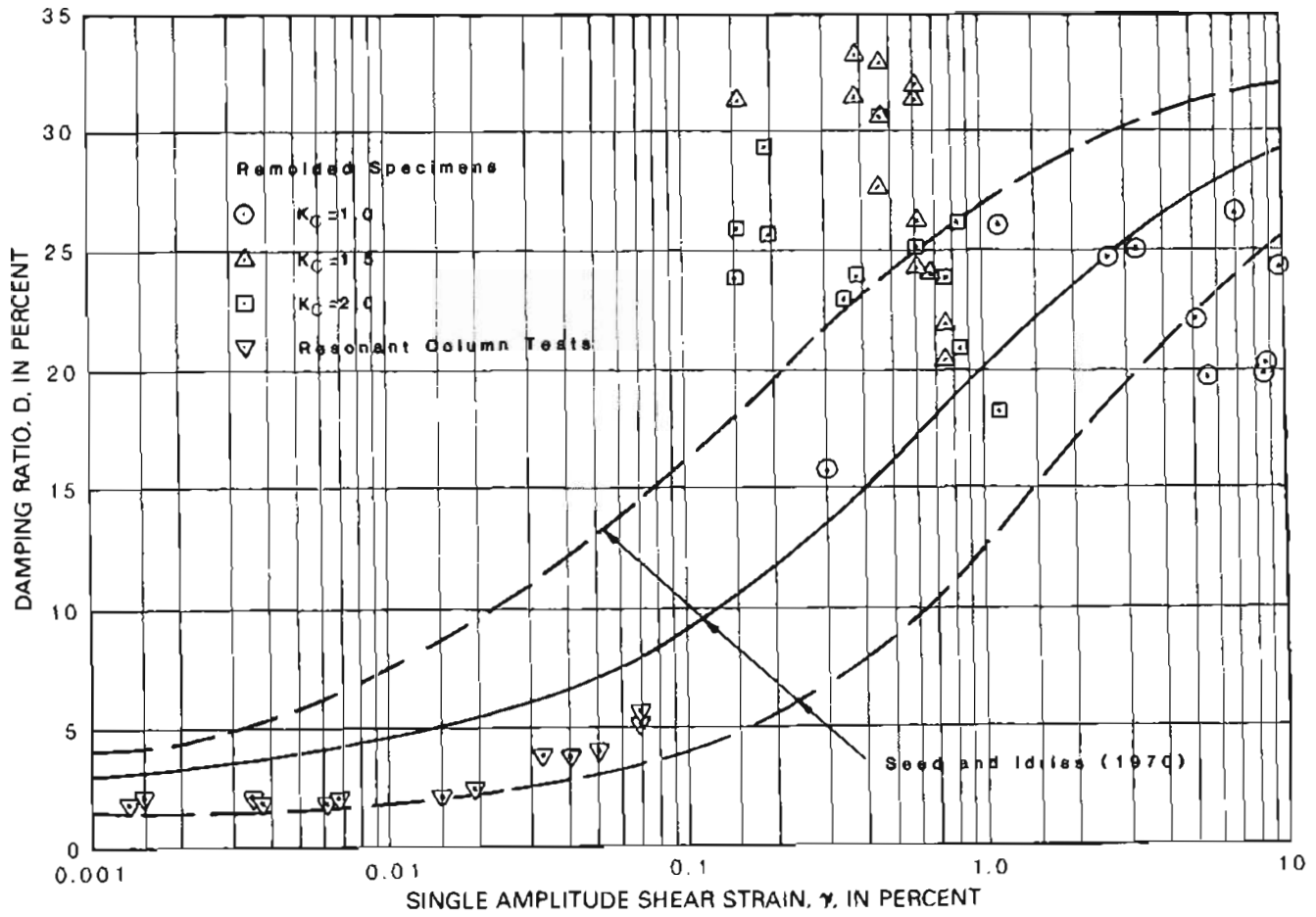


Figure 47. Damping ratios versus percent strain for remolded specimens tested at various consolidation ratios. Damping ratio curves from Seed and Idriss (1970) and data points from resonant column tests (Updike and others, 1982) are also shown.



